INTERPRETING THE EFFECTIVE PERMEABILITY OF PORE NETWORK MODELS USING THE DIFFUSE SOURCE METHODOLOGY

A Thesis

by

SHERRY LIU

Submitted to the Office of Graduate and Professional Studies of
Texas A&M University
in partial fulfillment of the requirements for the degree of

MASTER OF SCIENCE

Chair of Committee,	Michael J. King
Committee Members,	I. Yucel Akkutlu
	Juan Carlos Laya
Head of Department,	Jeff Spath

May 2019

Major Subject: Petroleum Engineering

ABSTRACT

The pore network model obtained from a micro-CT scan of a carbonate outcrop sample has been previously analyzed by former students of the research group for the effective permeability. Analysis techniques included steady state (face), well test derivative and depth of investigation methods. There existed a significant variation in the results from the different methodologies for the same pore network. For example, the results of the carbonate model in the Z-direction ranged from 1,219 md to 36,200 md. The focus of this research work is to find, apply and evaluate alternative methods to explain the large variation seen in the prior methods.

Pulse decay and diffuse source approaches were evaluated, where the diffuse source method was eventually chosen due to its ability to capture the range of transient effective transmissibility with respect to time. This method is used in upscaling and modifications are made for its application to the lattice grid. The method is based on a pseudo steady state approach and utilizes the concept of drainage volume. Drainage volume increase with time and the geometry of the increase is based on the diffusive time of flight of each pore within the pore network.

The method was applied to both a sandstone and a carbonate pore network. A homogeneous synthetic pore network was created to illustrate the expected differences between the lattice and analytical calculations of the diffuse source method. The comparison of the lattice and analytical solutions for each pore network can indicate the level of heterogeneity within the pore network. As expected, the sandstone model is

relatively homogeneous compared to the carbonate model. The variation of permeability values previously calculated is explained as a transient effect. On top of describing the internal heterogeneity, the method can also indicate the level of anisotropy due to the direction of flow. Finally, we are able to visualize the drainage pattern and the sub volumes that contribute to the transient transmissibility calculation.

DEDICATION

To my parents and husband for their love, support and encouragement along this journey.

ACKNOWLEDGEMENTS

I would like to express my gratitude to my committee chair, Dr. King, for his continuous support and patience during my research. He has guided me along the path of research and thesis writing. I would also like to thank my committee members, Dr. Akkutlu and Dr. Laya, for their support throughout the course of this research.

I would like to express my gratitude to Dr. Masa Prodanovic from University of Texas at Austin for kindly providing the sandstone model utilized for this research work. I would like to thank her graduate student Rui Xu for helping with the model transferring process. I would also like to thank Dr. Anuj Gupta's research group from Texas A&M University at Qatar for providing us with the μ-CT scan of the carbonate core utilized in this research work.

Finally, I would like to express my gratitude to the MCERI (Model Calibration and Efficient Reservoir Imaging) consortium and Energi Simulation (formerly Foundation CMG) for funding my research. I also want to thank members of the MCERI research group for sharing their knowledge about research and life.

CONTRIBUTORS AND FUNDING SOURCES

Contributors

This work was supervised by a thesis committee consisting of Dr. Michael King and Dr. Yucel Akkutlu of the Department of Petroleum Engineering and Dr. Juan Carlos Laya of the Department of Geology.

All work conducted for the thesis was completed by the student independently. Some of the Matlab codes are altered and built upon existing codes in the research group for consistency.

Funding Sources

The graduate study was partially supported by a fellowship from Texas A&M University. This work was also made possible in by graduate research assistantship from the MCERI consortium and Energi Simulation.

NOMENCLATURE

Variables

Property	**Description**	**Unit of Measure**	**Conversion to SI**
A	Cross sectional area of the sample	mm^2	10^{-6} m^2
c_t	Compressibility	$1/psi$	$(1/6894.76)/Pa$
k	Sample permeability	mD	$0.9869233\times10^{-15} m^2$
k_b	Bond permeability	mD	$0.9869233\times10^{-15} m^2$
k_{DS}	Stabilized zone permeability	mD	$0.9869233\times10^{-15} m^2$
L	Length of the sample	mm	10^{-3} m
L_b	Bond length	μm	10^{-6} m
L_{ref}	Reference length of the sample	mm	10^{-3} m
L_{sD}	Length of the stabilized zone (dimensionless)	$[1]$	
Δp_{DS}	Diffuse source pressure drop	psi	$6894.76Pa$
p_i	Node pressure	psi	$6894.76Pa$
p_r	Pressure on the reference face	psi	$6894.76Pa$

q_f	Total flow rate on the outlet face	ft^3/day	$\left((0.3048)^3/24\right)m^3/hr$
r_n	Node radius	μm	10^{-6} m
r_b	Bond radius	μm	10^{-6} m
r_{LOD}	Distance at the limit of detectability	mm	10^{-3} m
t	Time	hr	hr
T_b	Bond transmissibility	$mD \cdot ft$	$(0.9869233)(0.3048)\times 10^{-15} m^3$
T_{DS}	Diffuse source transmissibility	$mD \cdot ft$	$(0.9869233)(0.3048)\times 10^{-15} m^3$
T_{PSS}	Pseudo Steady State transmissibility	$mD \cdot ft$	$(0.9869233)(0.3048)\times 10^{-15} m^3$
V_d	Drainage volume	μm^3	10^{-18} m^3
V_n	Node volume	μm^3	10^{-18} m^3
V_p	Pore volume of the sample	μm^3	10^{-18} m^3
Greek			
α	Diffusivity of the sample	ft^2/hr	$(0.3048)^2 m^2/hr$
α_b	Bond diffusivity	ft^2/hr	$(0.3048)^2 m^2/hr$
ϕ	Porosity of the sample	$[1]$	
$\delta\tau_b$	Bond diffusive time of flight	$\sqrt{hr}$	$\sqrt{hr}$

μ	Viscosity	cp	$0.001 Pa \cdot \sec$
τ	Diffusive time of flight	$\sqrt{hr}$	$\sqrt{hr}$
τ_{adj}	Diffusive time of flight of nodes adjacent to outlet nodes		
τ_{LOD}	Limit of detectability	$\sqrt{hr}$	$\sqrt{hr}$
τ_{ref}	Reference diffusive time of flight	$\sqrt{hr}$	$\sqrt{hr}$

Abbreviations

CAT	Computerized Axial Tomography
CT	Computed Tomography
DOI	Depth of Investigation
DS	Diffuse Source
DTOF	Diffusive time of flight
µ-CT	Microtomography
SS	Steady State
SSF	Steady State Face
PSS	Pseudo Steady State
WTD	Well Test Derivative

TABLE OF CONTENTS

Page

ABSTRACT ii

DEDICATION iv

ACKNOWLEDGEMENTS v

CONTRIBUTORS AND FUNDING SOURCES vi

NOMENCLATURE vii

TABLE OF CONTENTS x

LIST OF FIGURES xii

LIST OF TABLES xvi

CHAPTER I INTRODUCTION 1

1.1 Digital Rocks 1
1.2 Carbonate Reservoir Heterogeneity 3
1.3 Sandstone Pore Network Basic Information 7
1.4 Carbonate Pore Network Basic Information 8
1.5 Issues 11

CHAPTER II METHODOLOGY 13

2.1 Proposed Possible Solution Methods 13
2.2 Lattice Grid 14
2.3 Diffusive Time of Flight 19
2.4 Diffuse Source Methodology on a Lattice 23
2.5 Diffuse Source Analytical Equations 30
2.6 Discussion 32

CHAPTER III RESULTS AND CONCLUSIONS 34

3.1 Synthetic Pore Network Model Results 34
3.2 Sandstone Pore Network Model Results 38
3.3 Carbonate Pore Network Model Results 43
3.5 Conclusions and Recommendations for Future Work 48

REFERENCES 50

APPENDIX A ANALYTICAL EQUATIONS FOR POINT NODE REPRESENTATION 58

APPENDIX B SANDSTONE PORE NETWORK MODEL RESULTS 60

APPENDIX C CARBONATE PORE NETWORK MODEL RESULTS 67

LIST OF FIGURES

Page

Fig. 1 – A Photograph of the Jebel Fuwairit Beach Bar Complex (Pasumarti, 2014) 8

Fig. 2 – The Whole Core (left) and Pore Network Utilized (right) of the Carbonate Pore Network Model (Pasumarti, 2014).....9

Fig. 3 – Sketches Representing the Steady State, Well Test Derivative and Depth of Investigation Methods 10

Fig. 4 – The Basic Component of the Lattice Grid for Pore Networks Consist of a Pair of Nodes and a Bond.....15

Fig. 5 – Coordination Number Comparison Between Carbonate and Sandstone Models (Liu and King, 2019). Reprinted with permission of Society of Petroleum Engineers.....16

Fig. 6 – Node Radius Comparison Between Carbonate and Sandstone Models (Liu and King, 2019). Reprinted with permission of Society of Petroleum Engineers. 17

Fig. 7 – Bond Radius Comparison Between Carbonate and Sandstone Models (Liu and King, 2019). Reprinted with permission of Society of Petroleum Engineers. 18

Fig. 8 – Bond Length Comparison Between Carbonate and Sandstone Models (Liu and King, 2019). Reprinted with permission of Society of Petroleum Engineers. 18

Fig. 9 – Illustration of an Example Lattice Pore Network to Explain the Diffuse Source Method (Liu and King, 2019). Reprinted with permission of Society of Petroleum Engineers.....21

Fig. 10 – A Step by Step Illustration of Dijkstra's Algorithm (Liu and King, 2019). Adapted with permission of Society of Petroleum Engineers. 22

Fig. 11 – An Illustration of the Concept of Drainage Volume (Liu and King, 2019). Reprinted with permission of Society of Petroleum Engineers.....26

Fig. 12 – Comparison of Drainage Volume Fraction Between Lattice and Analytical Calculations for the Point Node Formulation.....28

Fig. 13 – Drainage volume fraction and normalized transmissibility for the analytic linear solution (Liu and King, 2019). Reprinted with permission of Society of Petroleum Engineers.....32

Fig. 14 – LsD Comparison Between Lattice and Analytical for the Synthetic Pore Network 35

Fig. 15 – Transmissibility Comparison Between Lattice and Analytical for the Synthetic Pore Network.....36

Fig. 16 – LsD*Tds Comparison Between Lattice and Analytical for the Synthetic Pore Network.....36

Fig. 17 – Permeability Comparison for the Synthetic Pore Network.....37

Fig. 18 – Diagnostic Plot for the Synthetic Pore Network.....38

Fig. 19 – LsD Comparison Between Lattice and Analytical for the Two Faces in the X Direction of the Sandstone Pore Network 40

Fig. 20 – Transmissibility Comparison for the Two Faces in the X Direction of the Sandstone Pore Network.....40

Fig. 21 – Permeability Comparison for the Two Faces in the X Direction of the Sandstone Pore Network.....41

Fig. 22 – Diagnostic Plot for the X1 Face of the Sandstone Pore Network.....42

Fig. 23 – Diagnostic Plot for the X2 Face of the Sandstone Pore Network.....42

Fig. 24 – Drainage Patterns for the Two Faces in the X Direction of the Sandstone Pore Network (Liu and King, 2019). Reprinted with permission of Society of Petroleum Engineers.....43

Fig. 25 – LsD Comparison Between Lattice and Analytical for the Two Faces in the X Direction of the Carbonate Pore Network 45

Fig. 26 – Transmissibility Comparison for the Two Faces in the X Direction of the Carbonate Pore Network.....46

Fig. 27 – Diagnostic Plot for the X1 Face of the Carbonate Pore Network.....47

Fig. 28 – Diagnostic Plot for the X2 Face of the Carbonate Pore Network.....47

Fig. 29 – Drainage Patterns for the Two Faces in the X Direction of the Carbonate Pore Network (Liu and King, 2019). Reprinted with permission of Society of Petroleum Engineers....48

Fig. 30 – LsD Comparison Between Lattice and Analytical for the Two Faces in the Y Direction of the Sandstone Pore Network....60

Fig. 31 – Transmissibility Comparison for the Two Faces in the Y Direction of the Sandstone Pore Network....61

Fig. 32 – Permeability Comparison for the Two Faces in the Y Direction of the Sandstone Pore Network....61

Fig. 33 – Diagnostic Plot for the Y1 Face of the Sandstone Pore Network....62

Fig. 34 – Diagnostic Plot for the Y2 Face of the Sandstone Pore Network....62

Fig. 35 – Drainage Patterns for the Two Faces in the Y Direction of the Sandstone Pore Network....63

Fig. 36 – LsD Comparison Between Lattice and Analytical for the Two Faces in the Z Direction of the Sandstone Pore Network....63

Fig. 37 – Transmissibility Comparison for the Two Faces in the Z Direction of the Sandstone Pore Network....64

Fig. 38 – Permeability Comparison for the Two Faces in the Z Direction of the Sandstone Pore Network....64

Fig. 39 – Diagnostic Plot for the Z1 Face of the Sandstone Pore Network....65

Fig. 40 – Diagnostic Plot for the Z2 Face of the Sandstone Pore Network....65

Fig. 41 – Drainage Patterns for the Two Faces in the Z Direction of the Sandstone Pore Network....66

Fig. 42 – LsD Comparison Between Lattice and Analytical for the Two Faces in the Y Direction of the Carbonate Pore Network....67

Fig. 43 – Transmissibility Comparison for the Two Faces in the Y Direction of the Carbonate Pore Network....68

Fig. 44 – Diagnostic Plot for the Y1 Face of the Carbonate Pore Network....68

Fig. 45 – Diagnostic Plot for the Y2 Face of the Carbonate Pore Network....69

Fig. 46 – Comparison of the Two Y-Direction Faces' Anisotropy for the Carbonate Model 69

Fig. 47 – LsD Comparison Between Lattice and Analytical for the Two Faces in the Z Direction of the Carbonate Pore Network 70

Fig. 48 – Transmissibility Comparison for the Two Faces in the Z Direction of the Carbonate Pore Network 70

Fig. 49 – Diagnostic Plot for the Z1 Face of the Carbonate Pore Network 71

Fig. 50 – Diagnostic Plot for the Z2 Face of the Carbonate Pore Network 71

Fig. 51 – Comparison of the Two Z-Direction Faces' Anisotropy for the Carbonate Model 72

LIST OF TABLES

Page

Table 1 – Classification of Carbonate Rocks According to Depositional Texture (Dunham, 1962) 5

Table 2 – 15 Basic Carbonate Pore Types 6

Table 3 – Previous Permeability Results for the Fountainebleau Sandstone Sample 7

Table 4 – Permeability for the Carbonate Pore Network Calculated by Former Students 11

Table 5 – Basic Properties of Each Pore Network 20

Table 6 – The Number of Nodes Used by the Diffuse Source Method for Each Face for the Carbonate Model 24

Table 7 – The Number of Nodes Used by the Diffuse Source Method for Each Face for the Sandstone Model 24

Table 8 – Basic Properties for the Synthetic Pore Network 34

Table 9 – Permeability Comparison Between Different Methods for the Sandstone Model 39

Table 10 – Permeability Comparison Between Different Methods for the Carbonate Pore Network 44

CHAPTER I

INTRODUCTION

1.1 Digital Rocks

The modeling of porous media began with models as simple as sphere pack and bundle of tubes, which oversimplified and were not representative of the real pore network (Fatt, 1956). Fatt proposed a model where each pore space inside a rock was represented by a tube that initiated the modeling of pore networks.

The utilization of CT scans in the petroleum industry to model pore networks was the next big advancement. Although developed in 1972, X-ray computerized tomography was not used in petrophysics and reservoir engineering until the 1980s. CT scan images were able to capture the macroscopic immiscible displacement process, which provided a better understanding of oil recovery (Wang *et al.*, 1984). Properties such as porosity and fracture patterns could be extracted from the CT scan images, where the image capturing process could be completed within a minute (Wellington and Vinegar, 1987).

In 1987, microtomography was developed based on high-resolution X-ray tomography and the utilization of synchrotron X-ray source. This advancement in technology enabled the resolution of scanned images to approach 1 micrometer within 1% accuracy (Flannery *et al.*, 1987). The μ-CT technology was first applied to the petroleum industry to characterize porous media for Berea sandstone and synthetic beads (Dunsmuir *et al.*, 1991). Since the time consumption to create a 3D movie was too high, a small 2D

movie showing fluid displacement was created using the data from µ-CT scan taken at 5 second intervals.

A comparison of the CT and µ-CT scans for the same samples indicated that with the advantage of viewing pore networks at a higher resolution, µ-CT scan was able to capture more heterogeneity in pores, structural features and mineralogical distributions that was not possible with CT scan (Coles *et al.*, 1995). Next, medical axis was utilized as a tool to indicate the geometry of the void pathways inside porous media from images acquired from CT scans and the distributions of volumes of these void spaces were studied (Lindquist *et al.*, 1996). The high resolution µ-CT also enabled better visualization of 2D and 3D saturated core samples, where the data could be imported into flow simulators (Coles *et al.*, 1998).

In order to create a realistic pore network simulator, a thorough knowledge of the pore level physical processes and the pore formation processes was necessary (Bakke and Øren, 1997). A 3D sandstone model was generated with thin sections and the knowledge of the sedimentation, compaction and diagenesis processes. Due to the irregularity of the shapes of pores and pore throats, these elements were represented by the simplified geometries of spheres and cylinders of equal volumes to simulate fluid flow (Oren *et al.*, 1998). The same type of simplified representation has also been employed in this research work.

A lot of work has been completed on pore network modeling of multiphase flow with a focus on capillary pressure functions and relative permeabilities. These two properties are dependent on wettability, interfacial tension and the combination of viscous,

capillary and gravitational forces (Patzek, 2001). Compared to empirical relative permeability curves, physical based relative permeability curves generated using pore network models will lead to very different simulation results, especially for waterflood simulation (Blunt *et al.*, 2002).

The single-phase flow permeability of pore networks can be determined with Lattice-Boltzmann, Navier-Stokes or steady state flow simulation (Manwart, 2002; Mirabolghasemi *et al.*, 2015; Pasumarti *et al.*, 2015). This research work proposes a method to calculate the transmissibility and permeability of pore networks during the transient and PSS flow regimes.

1.2 Carbonate Reservoir Heterogeneity

Carbonate rocks are composed of calcite, magnesium calcite, aragonite and dolomite that are mostly formed in marine environments. The sediments of carbonate rocks are either precipitated or comes from skeletons inside their depositional environments (James and Jones, 2015).

Carbonate reservoirs are highly heterogeneous with a huge variation of pore types. The permeability can range in orders of magnitude from less than 1 md to more than 1000 md. The high heterogeneity of carbonates with pore sizes varying by orders of magnitude makes it more difficult to model compared to sandstone (Youssef *et al.*, 2007). The main reasons causing this heterogeneity include sedimentary fabrics, depositional environments, large scale and small-scale depositional cyclicity and, most importantly, diagenesis (MacDonald *et al.*, 2009). We will briefly discuss how carbonate rocks are

formed during deposition and how the diagenesis processes further contribute to the heterogeneity we see in carbonate rocks.

Most of carbonate sediments come from the skeletal remains of organisms in warm marine environments and at a depth within the photic zone. Some of the organisms' skeletal remains that form these sediments include microbes, algae, single cells, shells, echinoderms and colonial invertebrates.

The basic environments of deposition for carbonates include tidal flat, shallow shelf interior, shelf margin, slope and basin (Scholle *et al.,* 1983). The different environments of deposition have different weather conditions, water depth and organisms that dwell in them. Each environment of deposition is characterized by a unique combination of physical, chemical and biological processes leading to the formation of sediments of various sizes.

Carbonate diagenesis is driven by chemical disequilibrium between minerals and water, microbes, lithostatic pressure and hydrostatic pressure. The major processes of diagenesis include cementation, dissolution, dolomitization and fracturing.

Cementation occurs when carbonate crystals precipitate between carbonate sediments and can be triggered by falling temperature or increased hydrostatic pressure. Since they fill the pore spaces between sediments, this diagenesis process decreases existing porosity. Dissolution is when carbonate is dissolved by the surrounding water and is the reverse of precipitation. Thus, more pore spaces are created inside the carbonate rock by dissolution. Dolomitization happens when carbonate sediments or limestones transform partially or completely into dolomite. During this process, the texture and fabric

of the original rock are either partially or completely changed. Sometimes, the complete alteration of texture and fabric leads to increased porosity. Fracture development can result from extensional stress, compressional stress, faulting, folding, solution collapse, salt dome movement and overpressure. Fractures generate more porosity and serve as high permeability conduits (James and Jones, 2015).

Carbonate rocks can be classified by their texture into mudstone, wackestone, packstone, grainstone, boundstone and crystalline carbonates (Dunham, 1962). The distinctions of the classifications can be found in **Table 1**. Generally, the pore space within grain-supported textures are larger than the mud-supported textures.

<table>
<tr><td colspan="5">Depositional Texture Recognizable</td><td rowspan="3">Depositional Texture Recognizable

Crystalline Carbonate</td></tr>
<tr><td colspan="4">Original components not bond together during deposition</td><td rowspan="2">Original components bond together during deposition

Boundstone</td></tr>
<tr><td colspan="3">Contains mud</td><td rowspan="2">Lacks mud and is grain supported

Grainstone</td></tr>
<tr><td colspan="2">Mud supported</td><td rowspan="2">Grain supported

Packstone</td><td rowspan="2">Boundstone</td></tr>
<tr><td>Less than 10% grains

Mudstone</td><td>More than 10% grains

Wackestone</td><td></td><td></td></tr>
</table>

Table 1 – Classification of Carbonate Rocks According to Depositional Texture (Dunham, 1962)

The spaces between the grains or mud inside carbonate rocks make up the pore network. The primary pores of carbonates are formed at the time of deposition. As explained earlier, the diagenesis processes can have huge impacts on carbonates' permeability by creating secondary porosity or destroying porosity after primary deposition. Thus, the pores in carbonate rocks are highly heterogeneous and spatially correlated, leading to channeled flow along the high permeability streaks (Xu *et al.*, 1999).

The pores can be defined into 15 basic types and are listed in **Table 2** (Choquette and Pray, 1970).

Fabric Selective		Non Fabric Selective	Fabric Selective or Not
Inter-particle	Fenestral	Fracture	Breccia
Intra-particle	Shelter	Channel	Boring
Inter-crystal	Moldic	Vug	Burrow
Growth Framework		Cavern	Shrinkage

Table 2 – 15 Basic Carbonate Pore Types

Seven out of these fifteen types of porosities are most common and volumetrically abundant. They will be explained below (Choquette and Pray, 1970; James and Jones, 2015):

1. Inter-particle: the pore spaces between particles; depend on the size and packing of grains
2. Intra-particle: the pore spaces inside grains; depend on the skeletal architecture of bio-fragments
3. Intercrystal: pores between the constituent crystals; depend on the size, shape and packing of crystals
4. Moldic: formed as a result of preferential dissolution of components in limestone or dolostone
5. Fenestral: formed due to the decay of organic matter forming gas
6. Fracture: developed due to extensional or compressional stress, faulting, folding, solution collapse, salt dome movement and overpressure
7. Vug: developed due to bedrock dissolution and subsurface karst formation

Compared to autochthonous carbonates, sandstones are allochthonous (Ehrenberg and Nadeau, 2005). Carbonates' minerals are much more reactive than that of sandstone. There exist more modifications to carbonate porosity than sandstone porosity. Thus, carbonate pore networks are generally more heterogeneous than sandstone pore networks.

1.3 Sandstone Pore Network Basic Information

In order to evaluate a method's effectiveness, it is necessary to apply the method to more than one model and obtain reasonable results. To evaluate the rigorousness of the methodology chosen for this research work and provide outside comparison, we obtained a sandstone pore network model from Dr. Masa Prodanovic's research group at University of Texas in Austin.

This is the pore network of a Fountainebleau sandstone with porosity of 46%. Fountainebleau sandstones are from Paris Basin, France. They are Oligocene aged and composed of mostly quartz with some clay (Saadi *et al.*, 2017). The pore network is cubically shaped and measures 1.5mm on each side. The permeability previously evaluated by lab measurements and OpenFOAM are listed in **Table 3** (Kumar, 2009; Mirabolghasemi *et al.*, 2015).

Methodology	Permeability (Darcy)
Lab Measurement	3.0
OpenFOAM	2.6

Table 3 – Previous Permeability Results for the Fountainebleau Sandstone Sample

1.4 Carbonate Pore Network Basic Information

The micro-CT of a carbonate outcrop sample was provided to us by Dr. Anuj Gupta's research group from Texas A&M University at Qatar. The sample came from the Jebel Fuwairit Beach Bar Complex and a picture of this complex is shown in **Fig. 1**. It is a Holocene carbonate located in the northeast coast of Qatar. Their analysis showed that the Jebel Fuwairit carbonate samples collected consisted of lime-grainstone: skeletal and oolitic grains (Gupta and Poppelreiter, 2010).

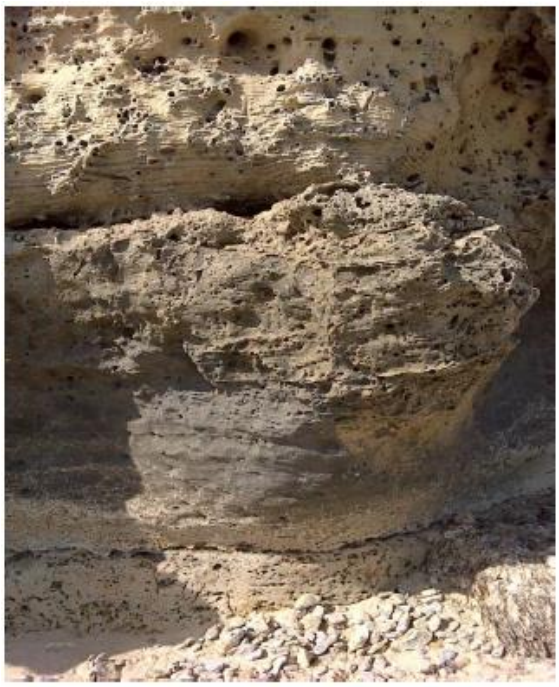

Fig. 1 – A Photograph of the Jebel Fuwairit Beach Bar Complex (Pasumarti, 2014)

Two former students in our research group conducted studies of this sample by extracting the pore network model with AVIZO FIRE suite and evaluating its permeability using MATLAB simulation. The core is approximately 12.4 mm in diameter and 14.1 mm

in length. The study by our research group was performed on a sub volume of this core that is rectangular shaped and measures approximately 7.5mm by 6.5 mm by 8.5 mm (**Fig. 2**).

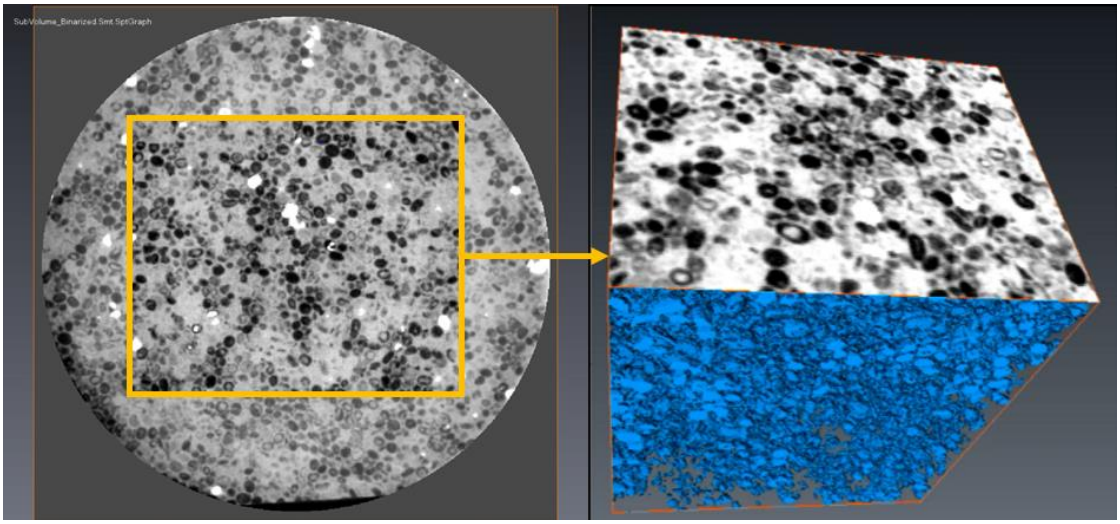

Fig. 2 – The Whole Core (left) and Pore Network Utilized (right) of the Carbonate Pore Network Model (Pasumarti, 2014)

Previous permeability evaluation methods conducted by our research group to analyze this carbonate pore network model include steady state face, well test derivative and depth of investigation methods (Pasumarti, 2014; Sengupta, 2016). Illustrations are created for each technique (**Fig. 3**) to help explain the fundamental concepts behind each method.

The steady state face method calculates the permeability across a pore network with the assumption of constant flow rate through the pore network from one face to the opposite face over the entire length of the sample. A constant pressure drop is imposed across the sample. Then the flow rate going through the sample is calculated in order to evaluate permeability with Darcy's equation. For the well test derivative technique, the

line of pores along the center of the pore network act as a producing well. The well test derivative is computed and plotted on a diagnostic plot to identify the flow regimes. Equations for the appropriate flow regimes are then applied to calculate the permeability of the system. The depth of investigation method corresponds to the permeability when the pressure pulse reaches the plane opposite from the source plane, where the pressure pulse is initiated. The permeability is calculated by observing the length of time for the pressure pulse to travel across the pore network.

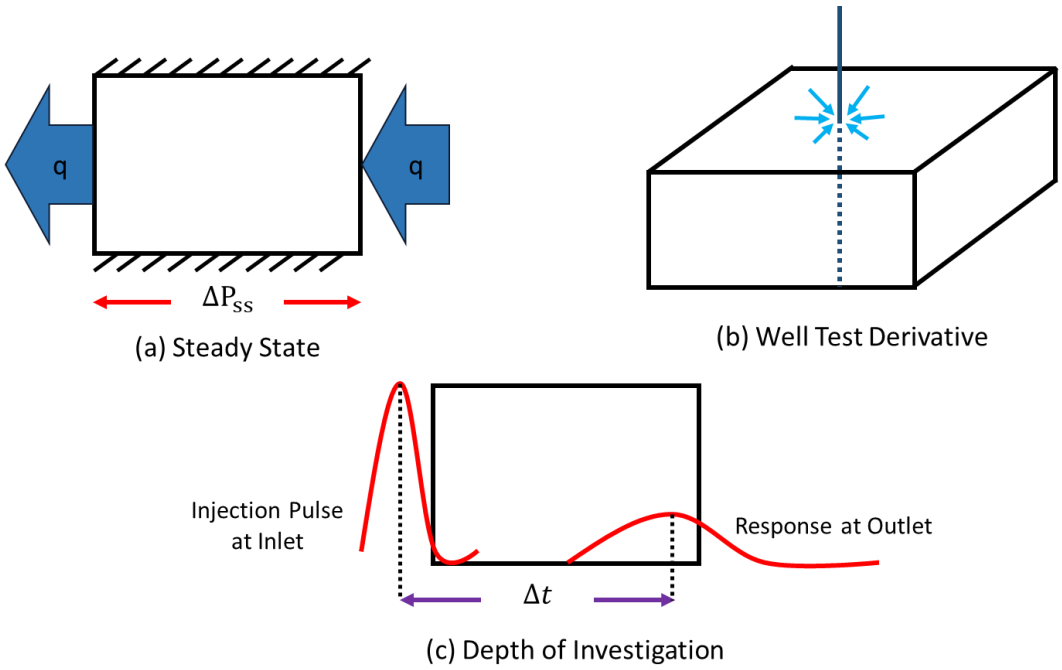

Fig. 3 – Sketches Representing the Steady State, Well Test Derivative and Depth of Investigation Methods

The results previously calculated for the carbonate model are listed in **Table 4** (Pasumarti, 2014; Sengupta, 2016). The geometric averages of planar permeability were calculated for the steady state and depth of investigation results in order to compare with

the line permeability calculated by the well test derivative method (Sengupta, 2016). The permeability values calculated using steady state and well test derivative methods are similar, but the result from the depth of investigation method is two orders of magnitude higher. The focus of this research work is to qualitatively and quantitatively explain the reason behind this wide spread of permeability values.

Direction	**Permeability (md)**					
	Steady State Face		Well Test Derivative		Depth of Investigation	
X	$\sqrt{k_y k_z}$	1,432	Line X	1,800	$\sqrt{k_y k_z}$	36,700
Y	$\sqrt{k_x k_z}$	1,290	Line Y	1,300	$\sqrt{k_x k_z}$	35,237
Z	$\sqrt{k_x k_y}$	1,516	Line Z	1,700	$\sqrt{k_x k_y}$	35,720

Table 4 – Permeability for the Carbonate Pore Network Calculated by Former Students

1.5 Issues

The motivation for this research work began with the curiosity of why the carbonate pore network permeability calculations performed using different methods varied in orders of magnitude. The problem was, on top of qualitatively explain the causes, how to quantitatively explain the variation. Once we were able to show quantitative results to explain the reason behind the wide spread permeability values, we wished to confirm the accuracy of the methodology employed. It was necessary to validate the methodology with results from works done by other research groups to provide an outside view. Thus, we applied the diffuse source method to the Fountainebleau sandstone model as validation. This diversified the scope of study from carbonate to silicate rock. The study was

performed keeping in mind the difference in heterogeneity between carbonates and sandstones geologically.

CHAPTER II

METHODOLOGY [*]

2.1 Proposed Possible Solution Methods

Two methods of evaluating permeability, pulse decay and diffuse source, were analyzed to possibly study the permeability of the pore network models described in the previous chapter. Pulse decay is a technique used in labs that calculate the permeability of a core based on transient flow. Diffuse source is an upscaling technique that can calculate the transmissibility during the transient and to the approximate pseudo steady state period (Nunna and King, 2017). I will describe both methodologies in more detail below and explain why the diffuse source method was finally chosen.

The pulse decay technique was originally derived to calculate the permeability of granite under high pressure (Brace *et al.*, 1968). The original equation derivations for this method made many assumptions. For example, the porosity of the rock and the transient due to temperature changes were assumed to be negligible. Some of the later work proposed analytical solutions with fewer assumptions (Hsieh *et al.*, 1981; Bourbie and Walls, 1982). As the technique was further expanded, even fracture properties could be determined using this transient technique (Ning *et al.*, 1993). In general, pulse decay technique utilizes transient flow to calculate permeability and is generally applied to

[*] Reprinted with permission from "Improved Calculation of Effective Permeability for Pore Network Models Using the Diffuse Source Methodology" by Sherry Liu and Michael J. King, 2019. Paper presented at the SPE Europec featured at the 81st EAGE Conference and Exhibition by The Society of Petroleum Engineers.

unconventional cores due to the lengthy time it would take for a steady state core flood. The method consists of an upstream and downstream reservoir in communication with the opposing faces of the core. A pressure pulse is initiated in the upstream reservoir by injecting a negligible volume of fluid. The differential pressure between the two reservoirs is recorded as time progress. Permeability is determined using the relationship between the differential pressure and time. A closer evaluation of this technique led to the conclusion that although the technique is transient, it can only calculate one permeability value and is unable to capture the permeability changes throughout this transient time period.

The diffuse source method was then analyzed, and the conclusion was this method can capture the change in effective transmissibility with respect to time and pore volume drained. The ability to see the permeability variation allow us to explain the range of permeabilities for the transient and pseudo steady state periods. The result of this method can explain the reason behind the large range of permeability values seen in the previous studies for the carbonate pore network. Thus, this method was chosen to be applied to the sandstone and carbonate pore networks.

2.2 Lattice Grid

All of the pore network models utilize a lattice grid to represent the pore networks. Instead of having six-faced cells in reservoir modeling, a lattice grid is made up of nodes and bonds as depicted in **Fig. 4**. This is the ball and stick model mentioned in Chapter I. The pores are represented by balls (nodes) while the pore throats are represented by sticks (bonds). Each node may have none to many nodes connected to it.

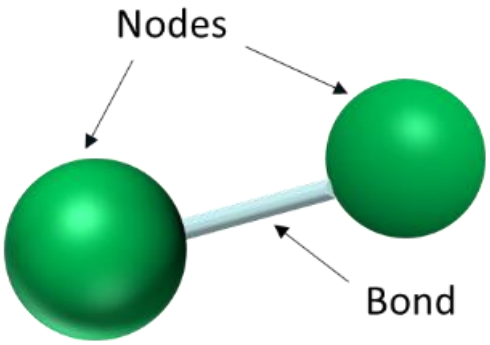

Fig. 4 – The Basic Component of the Lattice Grid for Pore Networks Consist of a Pair of Nodes and a Bond

The nodes contain all the volumes and the bonds serve as a transportation device to move the volumes between nodes. The flow between two connected nodes is represented by the Hagen-Poisuille equation (**Eq.1**). This equation assumes flow due to pressure differential across a tube at steady-state (Mani and Mohanty, 1998). From the Hagen-Poisuille equation, we can calculate the inter-node permeability and transmissibility**.**

$$q = \frac{\pi r_b^4}{8\mu L_b}\Delta p = \frac{1}{\mu}T_b \cdot \Delta p \qquad 1$$

$$k_b = \frac{1}{8}r_b^2 \qquad 2$$

The volumes of nodes are calculated using the radii inscribing the spherical nodes.

$$V_p = \frac{4}{3}\pi r_n^3 \qquad 3$$

Knowing the basic properties that makeup the lattice pore network, it is important to first take a look at the coordination number distribution, which shows the number of

connections each node has (**Fig. 5**). Compared to the sandstone pore network, the carbonate pore network has more nodes with coordination number on both extreme high and low ends. This means the internal connectivity inside the carbonate pore network is more complex.

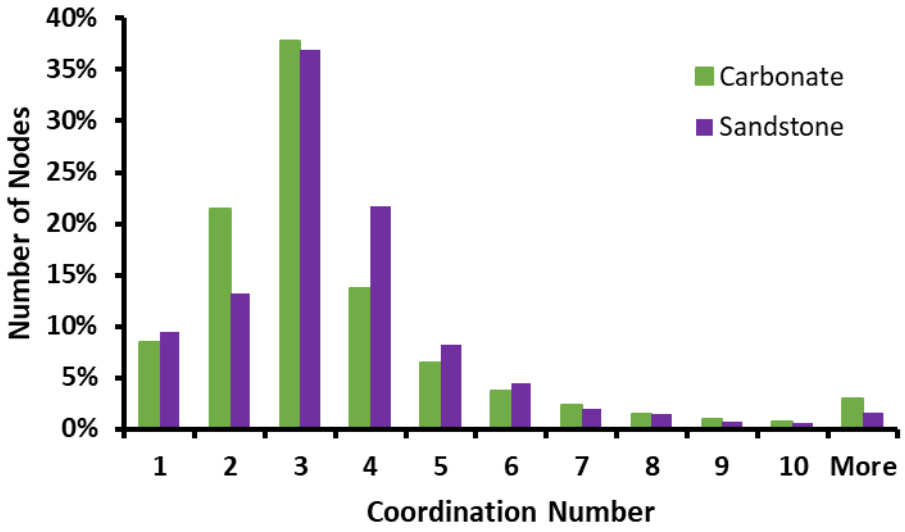

Fig. 5 – Coordination Number Comparison Between Carbonate and Sandstone Models (Liu and King, 2019). Reprinted with permission of Society of Petroleum Engineers.

The bond radius, bond length and node radius are the basic elements that make up a pore network. The distributions of these properties for the sandstone and carbonate pore networks are shown in **Fig. 6** through **Fig. 8**. Node radius directly affect the pore volumes of each pore network. The distribution of this property for the carbonate and sandstone models are very similar with the carbonate having more nodes of high radii.

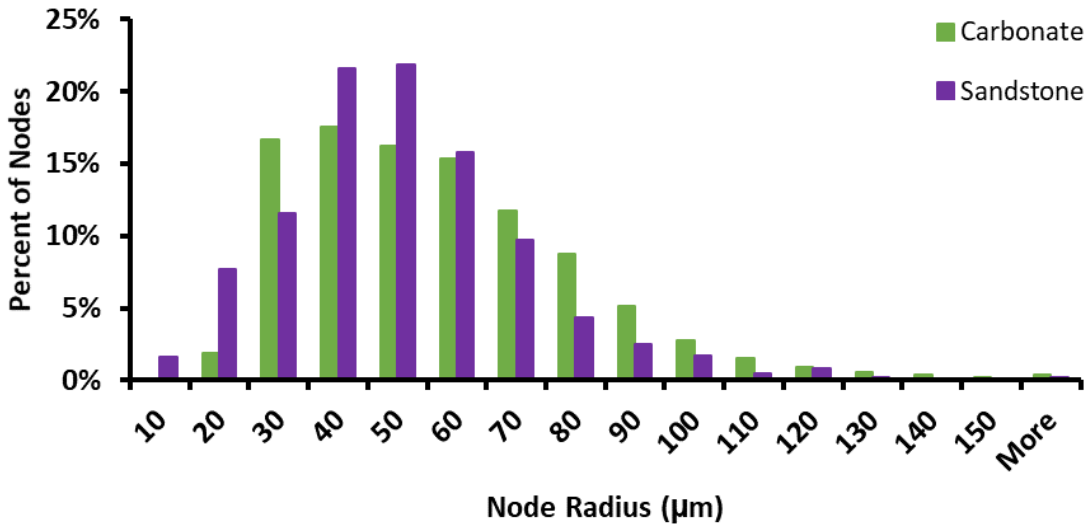

Fig. 6 – Node Radius Comparison Between Carbonate and Sandstone Models (Liu and King, 2019). Reprinted with permission of Society of Petroleum Engineers.

Bond radius effect the inter node permeability and transmissibility properties. The carbonate pore network has more bond of smaller radii, which means the flow is more restricted. The bond length impacts the inter node transmissibility and the distribution for the two models are completely different. The carbonate model appears to have a bimodal distribution, while the sandstone model has a unimodal distribution.

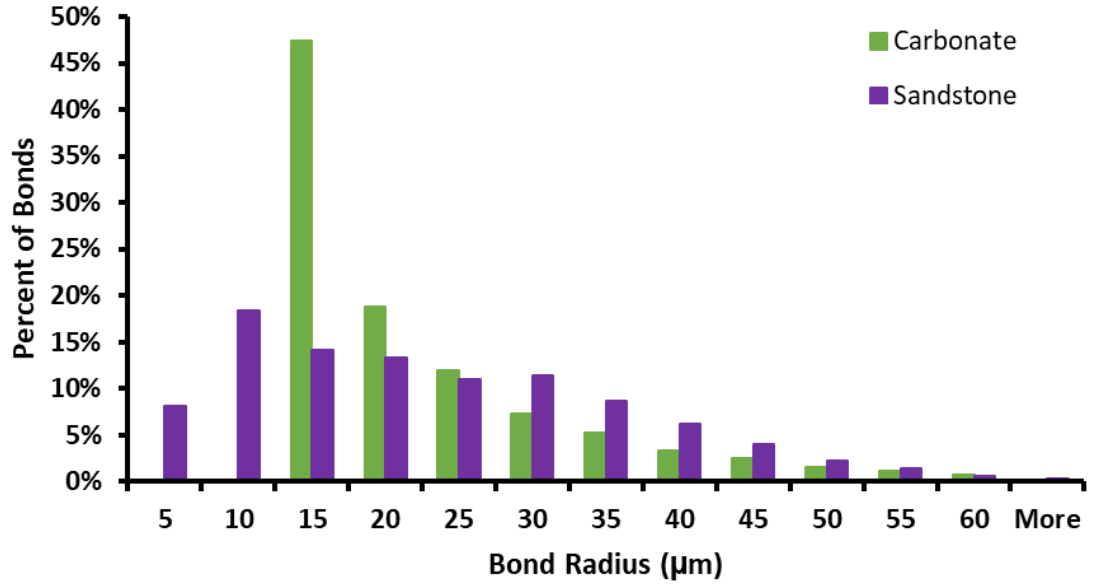

Fig. 7 – Bond Radius Comparison Between Carbonate and Sandstone Models (Liu and King, 2019). Reprinted with permission of Society of Petroleum Engineers.

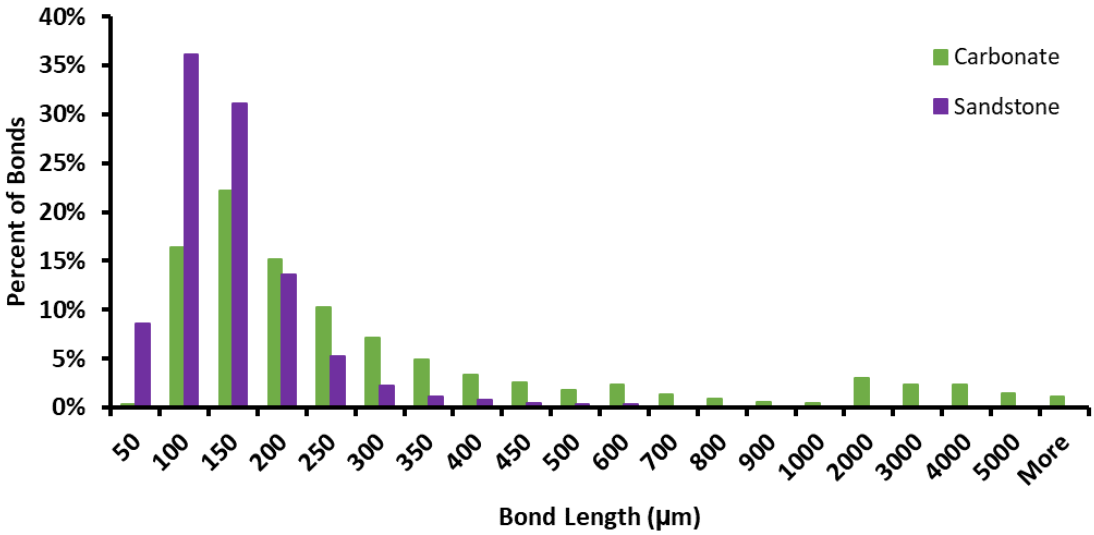

Fig. 8 – Bond Length Comparison Between Carbonate and Sandstone Models (Liu and King, 2019). Reprinted with permission of Society of Petroleum Engineers.

2.3 Diffusive Time of Flight

The proposed method uses the concept of the diffusive time of flight, which comes from the Eikonal equation. The Eikonal equation arises from the high frequency limit of the Fourier transform of the diffusivity equation, **Eq.4** (Virieux *et al.*, 1994; Vasco and Datta-Gupta, 1999; Kulkarni *et al.*, 2001).

$$\nabla\tau\left(\vec{x}\right)\bullet\vec{\vec{k}}\left(\vec{x}\right)\bullet\nabla\tau\left(\vec{x}\right)=\phi\left(\vec{x}\right)\mu c_t \qquad 4$$

The DTOF represent the peak pressure pulse front distance from an impulse source or sink and serves as a spatial coordinate. When the medium is homogeneous, the pressure pulse wave front moves out circularly in 2D radial flow. The wave front follows the heterogeneity pattern for a heterogeneous medium.

The solution to the diffusive time of flight for a homogeneous medium is given by **Eq.5**. Here, the diffusivity is defined by **Eq.6**. Generally, the diffusivity is a function of position. For a lattice grid, it will depend upon bond (Liu and King, 2019).

$$\tau=\frac{r}{\sqrt{\alpha}} \qquad 5$$

$$\alpha=\frac{k}{\phi\mu c_t} \qquad 6$$

The viscosity and compressibility are uniform in our analysis (**Table 5**), and largely scale out from the equations. When we cite our results as a function of time in specific calculations, the properties will have an impact.

Property	Synthetic	Sandstone	Carbonate
Viscosity (cp)	1	1	0.2
Compressibility (psi^{-1})	$3X10^{-6}$	$3X10^{-6}$	$3X10^{-5}$

Table 5 – Basic Properties of Each Pore Network

To calculate the diffusive time of flight on a lattice grid, it is necessary to first find the incremental diffusive time of flight across each of the bonds (**Eq.7**). Since the porosity of a bond is 1, it will not contribute to the calculation of the incremental DTOF across a bond.

$$\delta\tau_b = L_b\sqrt{\frac{\mu c_t}{k_b}} \qquad 7$$

Once $\delta\tau_b$ are found for all bonds, Dijkstra's algorithm is applied to find the diffusive time of flight for the entire pore network, starting with the τ of zero at the flowing face nodes at the outlet of the system, as shown in **Fig. 9**.

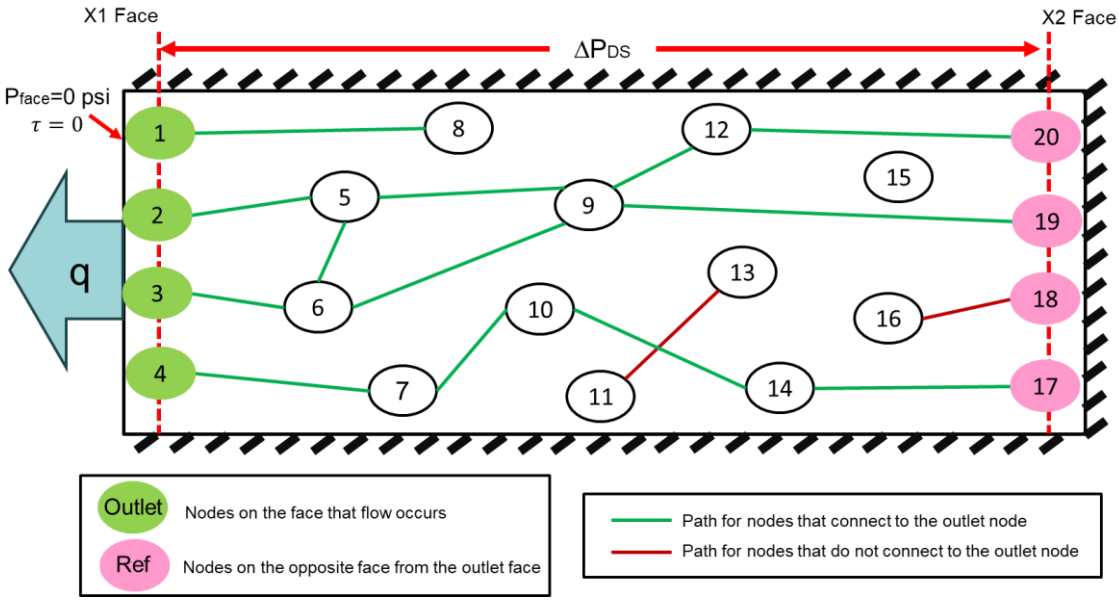

Fig. 9 – Illustration of an Example Lattice Pore Network to Explain the Diffuse Source Method (Liu and King, 2019). Reprinted with permission of Society of Petroleum Engineers.

Dijkstra's algorithm is a sequential algorithm that enables us to find the smallest value of τ from the outlet node to rest of the nodes in the pore network. Note that the nodes that cannot connect to the outlet nodes will have a τ of infinity, meaning they will never be drained. An illustration of Dijkstra's algorithm is shown in **Fig. 10** (Dijkstra, 1959; Cormen *et al.*, 2009).

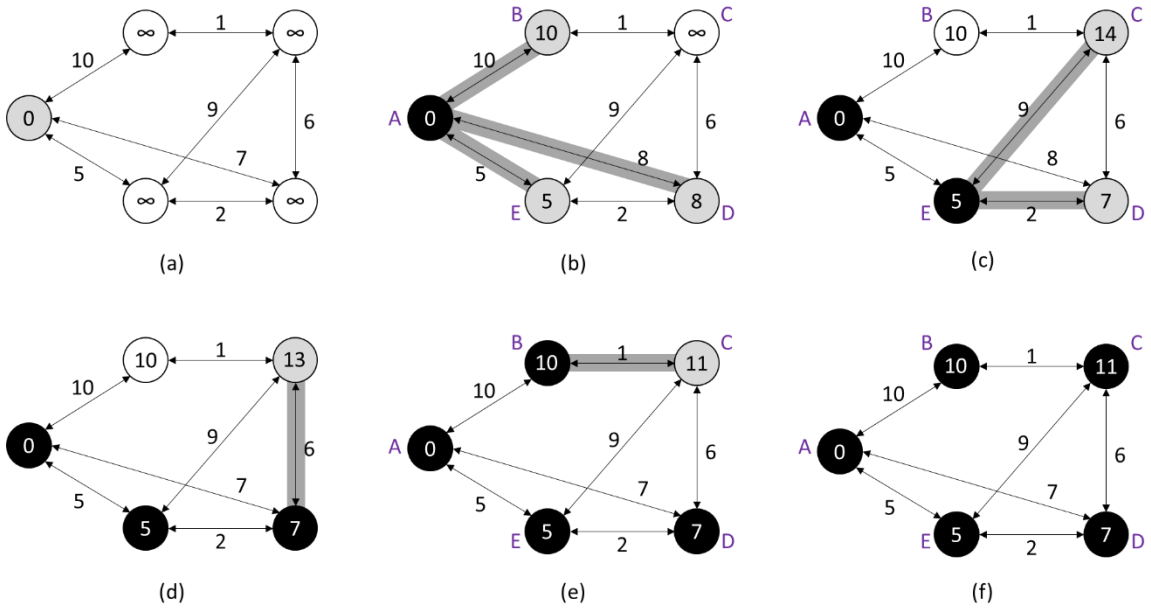

Fig. 10 – A Step by Step Illustration of Dijkstra's Algorithm (Liu and King, 2019). Adapted with permission of Society of Petroleum Engineers.

Below is an explanation of the steps in Dijkstra's algorithm using Fig. 10:

1. Begin by initiating the τ for the outlet node A with the value of zero and all other nodes with the value of infinity
2. Calculate the τ for all the nodes adjacent to node A by adding the incremental τ to the τ value of node A. If the newly calculated τ is smaller than the current τ, the newly calculated τ will be accepted
3. Find the node with the lowest τ (with the exclusion of node A) and calculate the τ of Node E's adjacent nodes
4. Find the node with the lowest τ (with the exclusion of node A and E) and calculate the τ of Node D's adjacent nodes
5. Repeat the above procedure until all the nodes are through

2.4 Diffuse Source Methodology on a Lattice

The diffuse source method was originally derived for pressure transient and production analysis in unconventional reservoirs and later utilized for upscaling work (King *et al.*, 2016; Nunna and King, 2017; Wang *et al.*, 2017). In its simplest form, it models pressure transients in a heterogeneous porous media for a fixed rate drawdown. For the lattice grid, we assume only one face of the pore network has a constant outflow rate and a pressure of zero, while all other faces are no flow boundaries (Fig. 9). The nodes on the face with outflow are labelled as outlet nodes while reference nodes are those on the opposite face from the outflow face. The differential pressure between the two faces is used to calculate the diffuse source transmissibility.

As mentioned earlier, not all the nodes within the pore network will connect to the outlet nodes. It is important to note that only those nodes in connection with the outlet nodes will be utilized for the diffuse source method. The nodes isolated from the outlet nodes, including reference nodes, will be excluded. The carbonate model has a total of 83,623 nodes and the sandstone model has 2,392 nodes. The total number of nodes, outlet nodes and reference nodes utilized to make the calculations for the two models are listed in **Table 6** and **Table 7**. The number of nodes used for the carbonate pore network calculation were different for all faces. The number of nodes used for the different faces for the sandstone model remained relatively constant. This is probably due to the sample size difference of the pore networks and the fact that the sandstone pore network is more homogeneous.

Face	Number of Nodes		
	Used for Calculation	Outlet	Reference
X1	80,478	1,469	1,653
X2	80,401	1,683	1,383
Y1	80,562	1,708	1,790
Y2	80,447	1,865	1,568
Z1	80,418	1,340	1,614
Z2	80,408	1,648	1,292

Table 6 – The Number of Nodes Used by the Diffuse Source Method for Each Face for the Carbonate Model

Face	Number of Nodes		
	Used for Calculation	Outlet	Reference
X1	2,234	40	45
X2	2,236	47	39
Y1	2,234	42	37
Y2	2,236	39	41
Z1	2,232	47	45
Z2	2,232	45	47

Table 7 – The Number of Nodes Used by the Diffuse Source Method for Each Face for the Sandstone Model

Eq.8 is the general equation for the diffuse source methodology (King *et al.*, 2016).

$$\nabla \cdot \vec{u} = \frac{q_{face}}{V_d(t)} \phi e^{-\tau^2/4t} \qquad 8$$

This approximation to the solution of the diffusivity equation allows us to treat time as a parameter. For many of the reference solutions utilized in pressure transient analysis, this approximation is exact (Lee, 1982). Once discretized on the lattice we have

the following sparse matrix equation, where j is summed over all nodes connected to node i (Liu and King, 2019).

$$\frac{1}{\mu}\sum_{node,j} T_{ij}\cdot\left(p_i - p_j\right) = \frac{q_f}{V_d\left(t\right)} V_{n,i}\cdot e^{-\tau_i^2/4t} \qquad 9$$

An important concept behind the diffuse source method imbedded in Eq.9 is drainage volume, which is defined by **Eq.10**. Here V_n is the pore volume of each node. The exponential term inside this equation indicate the percentage contribution of each node to the total production due to fluid expansion.

$$V_d\left(t\right) = \sum_{node,i} V_{n,i}\cdot e^{-\tau_i^2/4t} \qquad 10$$

Drainage volume is time dependent and increase with time until PSS is reached (**Fig. 11**). When the time is small compared to a node's τ, the exponential term in Eq.10 approaches zero, which means the node is barely making any contribution to the drainage volume calculation. On the other hand, when the time is large compared to a node's τ, the exponential term approaches one, meaning the node is contributing 100% to the fluid production and has reached PSS. When the entire pore network is depleted, the pore network is said to have reached PSS.

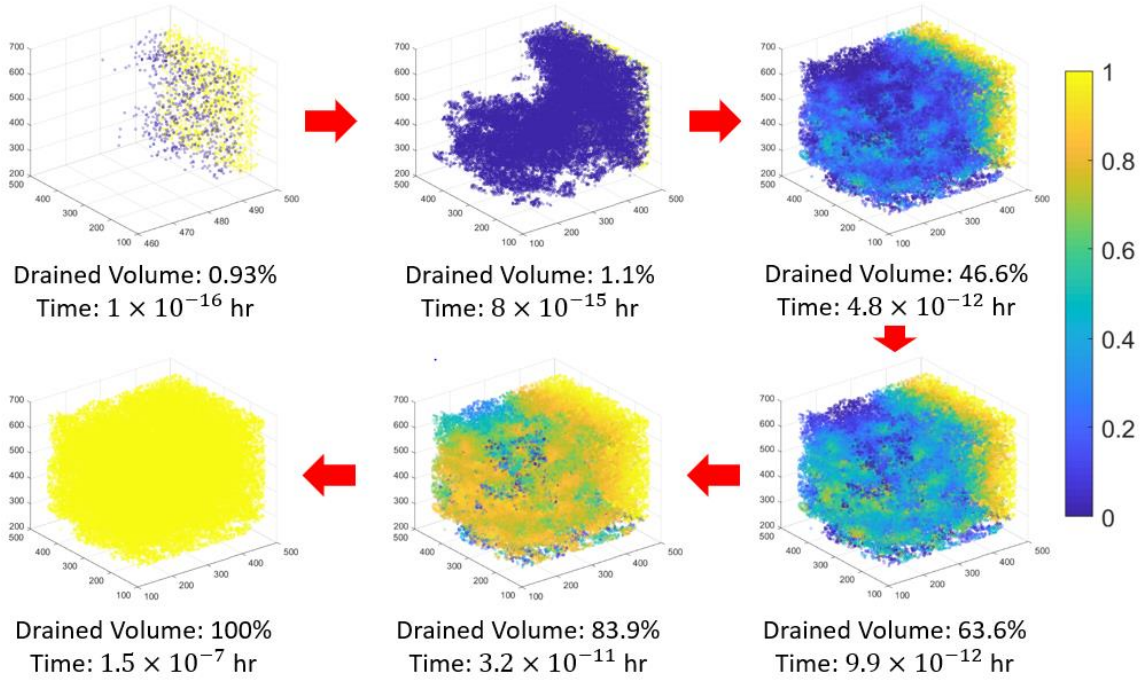

Fig. 11 – An Illustration of the Concept of Drainage Volume (Liu and King, 2019). Reprinted with permission of Society of Petroleum Engineers.

The drainage volume fraction, or the (dimensionless) length of the stabilized zone, can be calculated with **Eq.11** (Lee, 1982). It represents the percentage of the pore network that is currently drained.

$$L_{sD} = V_d(t)/V_p = r_{LOD}/L_{ref} \tag{11}$$

$$V_p = \sum_{nodes,i} V_{n,i} \tag{12}$$

$$L_{ref} = \sum_{i:ref} V_{n,i} \cdot x_i \Big/ \sum_{i:ref} V_{n,i} - \sum_{i:flow} V_{n,i} \cdot x_i \Big/ \sum_{i:flow} V_{n,i} \tag{13}$$

In Fig. 11, at early time when 0.93% of the total pore network volume was drained, the nodes on the outflow face are at PSS and only a small number of nodes inside the pore network started to be drained. With increasing time, the drained volume increased to 1.1%

and more nodes within the pore network began to contribute to the drainage volume. Eventually, all the nodes started to contribute to the drainage volume. At 63.6% drained volume, there appeared to be some yellow streaks that reached the reference face. These represented high permeability paths that first reached the reference face. Eventually, the entire pore network reached PSS.

The pressure front reaches nodes with lower τ before effecting the ones with higher τ. Therefore, the path with highest permeability will tend to have lowest τ values for the nodes along this path. The areas that are last fully drained consist of nodes with the largest τ values.

Once the pressures for all the nodes are solved for a specific time, the pressure on the reference face is calculated (**Eq.14**). Since the pressure on the outflow face is set to zero, the pressure on the reference face is essentially the pressure drop across the pore network.

$$\Delta p_{DS}(t) = p_r(t) = \sum_{nodes,j} p_j(t) \cdot V_{n,j} \Big/ \sum_{nodes,j} V_{n,j} \tag{14}$$

Next, the transmissibility across the pore network can be found using the pressure drop across the pore network.

$$T_{DS}(t) = \frac{\mu q_f}{\Delta p_{DS}(t)} \tag{15}$$

However, we notice that using the above point node formulation, the lattice and analytical results showed a time lag in drainage volume (**Fig. 12**). The analytical equations for point node formulation can be found in Appendix A. Therefore, the determination of

drainage volume and transmissibility, thus the effective permeability, require additional specification.

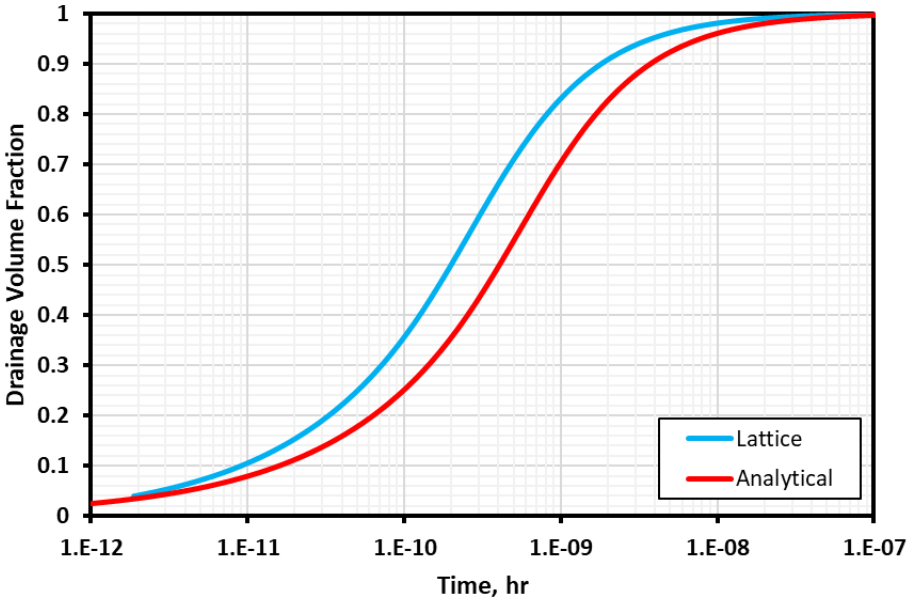

Fig. 12 – Comparison of Drainage Volume Fraction Between Lattice and Analytical Calculations for the Point Node Formulation

Two modifications to the point node form of the diffuse source method are necessary. The first modification improves the correspondence between the analytic reference solution and the lattice calculations, especially at early time, by replacing the point nodes with linear elements. This idea is very similar to a method that was used to improve the early time response of discretized models for welltest interpretation (Li, C.K., Michael J., 2016). A minimum and a maximum τ value for each linear element (i) is calculated with the τ of the node itself and the adjacent nodes (j). This is equivalent to

defining the value of τ for any bond as the average on the adjacent nodes. For the outlet nodes, the minimum τ would be zero (Liu and King, 2019).

$$\tau_i^{Min} = \frac{1}{2} \cdot \left(\tau_i + Min\left(\tau_i, \left\{ \tau_j \right\} \right) \right) \tag{16}$$

$$\tau_i^{Max} = \frac{1}{2} \cdot \left(\tau_i + Max\left(\tau_i, \left\{ \tau_j \right\} \right) \right) \tag{17}$$

The second modification has also been utilized in Diffuse Source upscaling (Liu *et al.*, 2019). The specific form of the exponential term in Eq.10 is a consequence of the Eikonal equation and the high frequency limit of the diffusivity equation. It provides an accurate approximation of the pressure transient solutions, especially at early time. However, for the purpose of an upscaling calculation, it is instead simpler and more accurate to replace the source term with a PSS solution on a sub-volume given by the limit of detectability, (Malone *et al.*, 2019).

$$\tau_{LOD} = \sqrt{16t} = 4\tau_{ref}\sqrt{t_D} \tag{18}$$

$$\tau_{ref} = \sum_{i:ref} V_{n,i} \cdot \tau_i \Big/ \sum_{i:ref} V_{n,i} \tag{19}$$

For values of τ beyond the limit of detectability, $e^{-\tau^2/4t} \le 0.018$, and there is a negligible contribution to the drainage volume. In this simplified representation, the source term is replaced by the PSS limit for $\tau < \tau_{LOD}$ and 0 for $\tau \ge \tau_{LOD}$. Combining this simplification with the definition of the linear element, we make the following replacement for the source term.

$$e^{-\tau_i^2/4t} \to Max\left(0, Min\left(1, \frac{\tau_{LOD} - \tau_i^{Min}}{\tau_i^{Max} - \tau_i^{Min}} \right) \right) \tag{20}$$

In order to obtain a reasonable transmissibility, the drainage volume has to drain more than just the flowing face nodes. Therefore, a minimum time limit is imposed using the τ of the nodes adjacent to the outlet nodes.

$$t_{\min} = \frac{\tau_{adj}^2}{16} \tag{21}$$

$$\tau_{adj} = \sum_{i:adj} V_{n,i} \cdot \tau_i \Big/ \sum_{i:adj} V_{n,i} \tag{22}$$

The effective permeability can then be calculated for samples that are relatively homogeneous with uniform drainage. For samples that are highly heterogeneous, early breakthrough to the opposite face may occur. Thus, our definition of limit of detectability is not representative. This completes the description of the diffuse source formulation, as adapted for calculations on a lattice.

$$k_{DS}(t) = \frac{r_{LOD}}{2A} T_{DS} = \frac{L_{ref}}{2A} L_{sD} \cdot T_{DS} \tag{23}$$

2.5 Diffuse Source Analytical Equations

A set of analytical equations for a homogeneous linear sample is derived from the linear element representation form of the diffuse source term. The calculated lattice PSS permeability is the analytical permeability of the sample. The PSS transmissibility calculated from the lattice will also serve as an input parameter. The porosity of the sample is found from the lattice by **Eq.24**.

$$\phi = V_p \big/ (L \cdot A) \tag{24}$$

The limit of detectability may be expressed as a distance, where it is limited to the length of the sample.

$$r_{LOD} = Min\left(L, \sqrt{\alpha}\tau_{LOD}\right) = Min\left(L, \sqrt{16\alpha t}\right) = L \cdot Min\left(1, \sqrt{16 t_D}\right) \quad 25$$

The drainage volume and the length of the stabilized zone can be expressed in terms of r_{LOD}.

$$V_d = A\phi r_{LOD} \quad L_{sD} = V_d / V_p = r_{LOD} / L \quad 26$$

We see that r_{LOD} is the length of the stabilized zone for this particular choice of the source function. We may also calculate the diffuse source flux profile within the sample, which is related to the pressure drop by Darcy's law.

$$q(r,t) = q_f \cdot Max\left(0, \frac{r_{LOD} - r}{r_{LOD}}\right) = \frac{kA}{\mu}\frac{\partial p}{\partial r} \quad 27$$

This leads to an expression for the pressure drop across the sample, and the transmissibility (Liu and King, 2019).

$$\Delta p_{DS}(t) = \frac{\mu q_f}{kA}\int_0^{r_{LOD}} dr\left(\frac{r_{LOD} - r}{r_{LOD}}\right) = \frac{\mu q_f}{kA}\frac{r_{LOD}}{2} \quad 28$$

$$T_{DS}(t) = \frac{\mu q_f}{\Delta p_{DS}} = \frac{2kA}{r_{LOD}} = \frac{2kA}{L}\frac{L}{r_{LOD}} = \frac{T_{PSS}}{L_{sD}} \quad 29$$

These solutions for the drainage volume fraction and the transmissibility normalized to the PSS value are shown in **Fig. 13**. Notice that the product of $L_{sD}(t) \cdot T_{DS}(t) = T_{PSS}$ is constant for this homogeneous analytical solution. Also, during

the period of the transient, $\Delta p_{DS}(t) = 2\frac{\mu q_f L}{kA}\sqrt{t_D}$, which has the expected scaling as the square root of time for infinite acting linear flow.

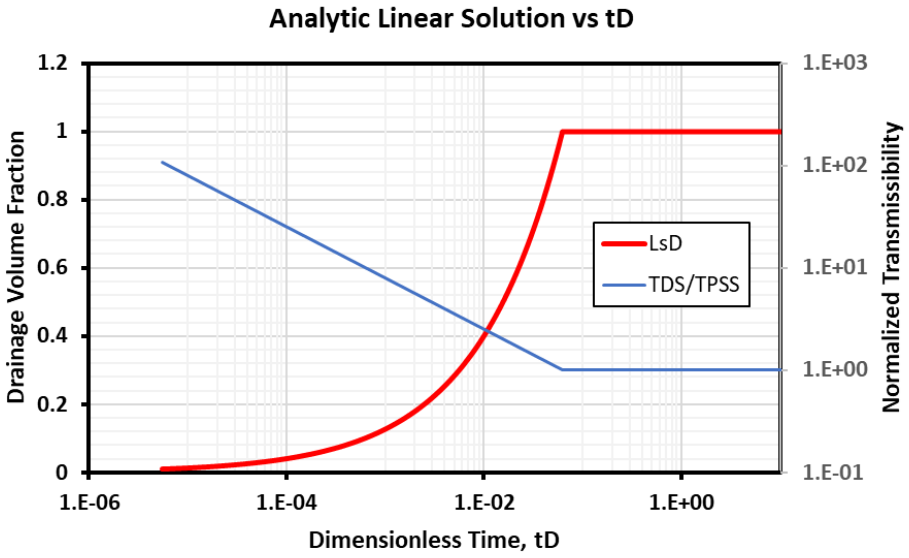

Fig. 13 – Drainage volume fraction and normalized transmissibility for the analytic linear solution (Liu and King, 2019). Reprinted with permission of Society of Petroleum Engineers.

The analytical expressions for the transmissibility and the drainage volume can be used as a reference solution to compare with the lattice solutions. Such a comparison can indicate the degree of internal heterogeneity of the pore network.

2.6 Discussion

Two methodologies have been studied in detail and the diffuse source method was eventually chosen to be applied to the carbonate and sandstone models. This will be the first attempt to apply this upscaling methodology to a lattice grid. Since this technique is

based on the drainage volume concept and drainage volume vary with time, a range of permeability values within the pore network could be captured.

Knowing that the carbonate model is more heterogeneous than the sandstone pore network model by examining their property distributions, we expected to see the diffuse source method to capture this difference in internal heterogeneity.

CHAPTER III

RESULTS AND CONCLUSIONS [*]

3.1 Synthetic Pore Network Model Results

A synthetic homogeneous lattice model consisting of 50 nodes and 49 bonds is created to illustrate how the lattice and analytical solutions should compare. The basic make up of this model are listed in **Table 8**.

Property	Value
Node Volume (μm^3)	523599
Bond Radius (μm)	20
Bond Length (μm)	200
Sample Length (μm)	10,000
Sample Area (μm^2)	40,000

Table 8 – Basic Properties for the Synthetic Pore Network

As shown in **Fig. 14**, the drainage volume fraction between the lattice and analytical nearly overlap at early time and completely overlaps at late time. This demonstrate that the linear element lattice result of diffuse source is able to capture the drainage pattern of the pore network with high accuracy.

[*] Reprinted with permission from "Improved Calculation of Effective Permeability for Pore Network Models Using the Diffuse Source Methodology" by Sherry Liu and Michael J. King, 2019. Paper presented at the SPE Europec featured at the 81st EAGE Conference and Exhibition by The Society of Petroleum Engineers.

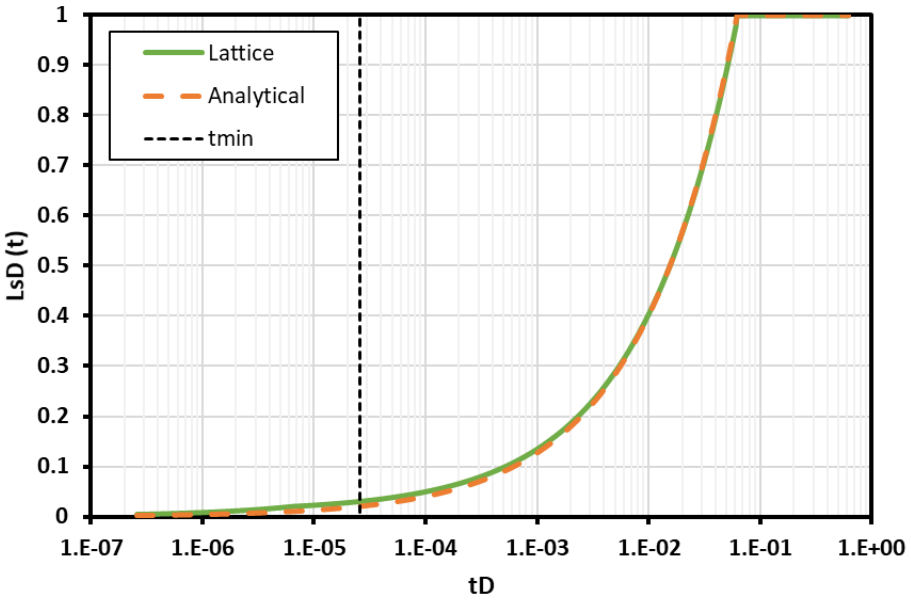

Fig. 14 – LsD Comparison Between Lattice and Analytical for the Synthetic Pore Network

Looking at the calculated diffuse source transmissibility (**Fig. 15**), we find that at time smaller than $t_{\min}$, transmissibility diverges and is unreasonably high. This shows the necessity of defining a minimum time. At approximately 10% drainage volume fraction, the lattice and analytical transmissibility almost overlap. The result becomes more accurate as more percentage of the pore network is utilized for the calculation.

We notice that $L_{sD} \cdot T_{DS}$ is constant for the analytical solution as expected (**Fig. 16**). The discretization causes the lattice result to be much higher at early time and becomes constant as a higher portion of the pore network is utilized for the calculation. The results between lattice and analytical overlaps at about 20% drainage volume fraction.

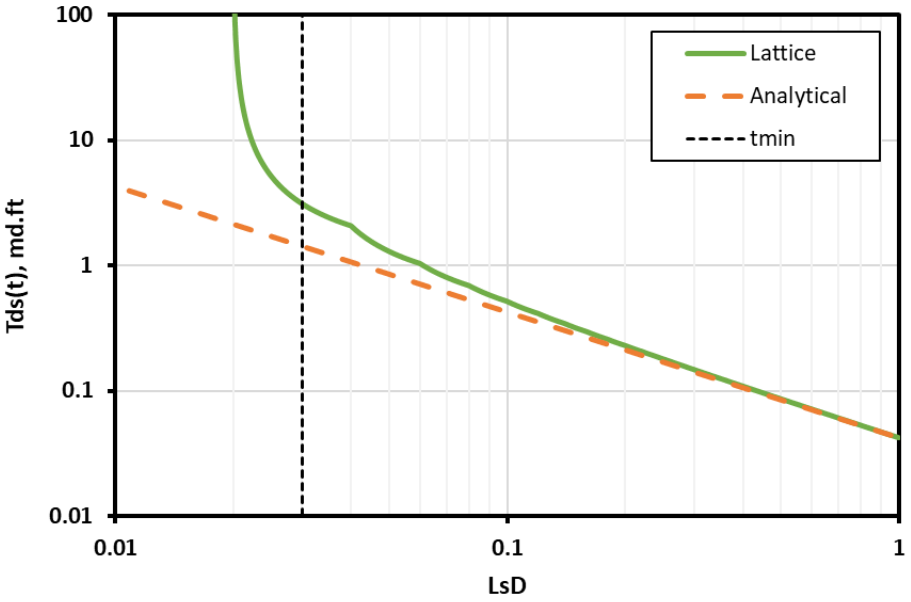

Fig. 15 – Transmissibility Comparison Between Lattice and Analytical for the Synthetic Pore Network

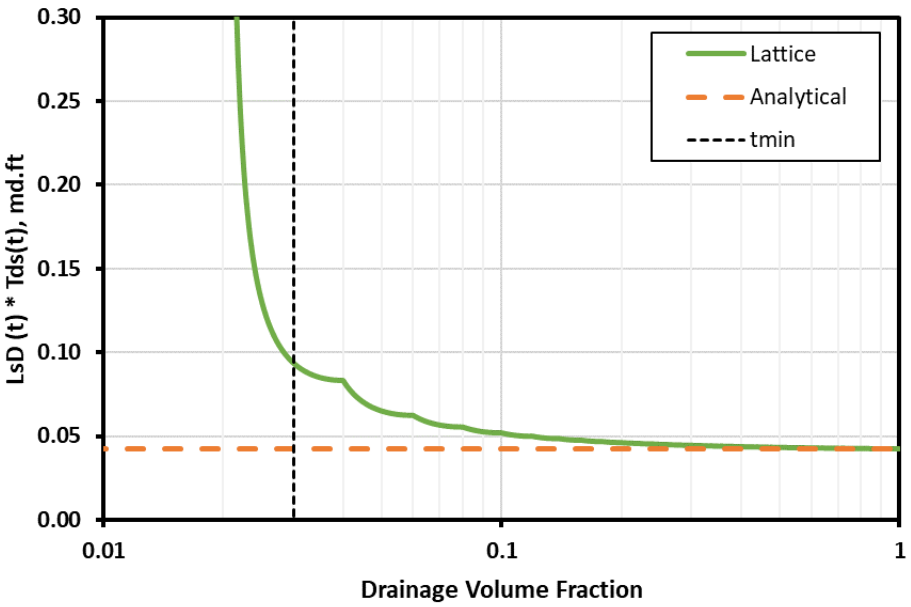

Fig. 16 – LsD*Tds Comparison Between Lattice and Analytical for the Synthetic Pore Network

Looking at the permeability comparison in **Fig. 17**, we see that the permeability of the lattice is extremely high at early time and relatively well matches the analytical result as the drainage volume fraction goes up to 20%.

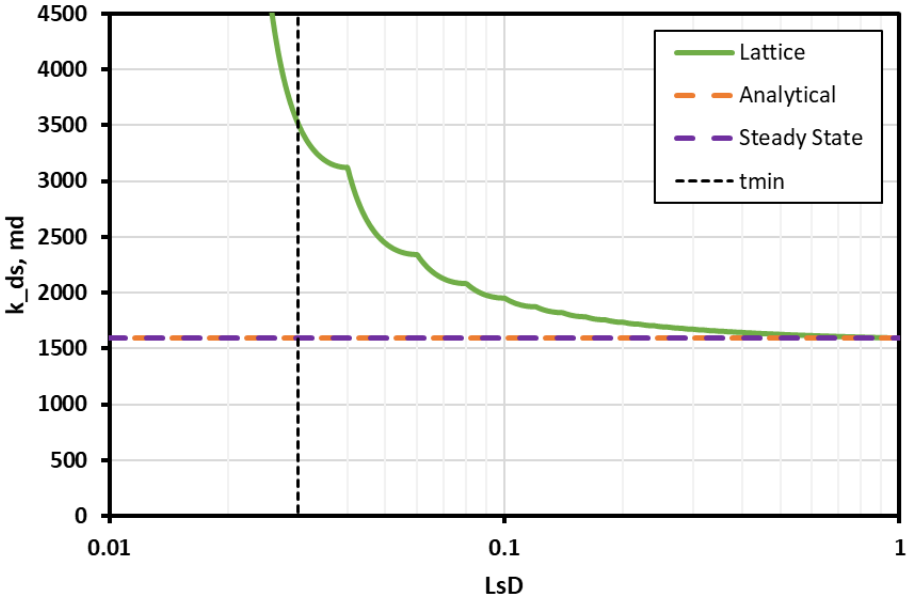

Fig. 17 – Permeability Comparison for the Synthetic Pore Network

Finally, the diagnostic plots between the lattice and analytical matches really well even at early time as long as we are above the minimum time (**Fig. 18**). We see that both the lattice and analytical results indicate the flow goes from linear to PSS flow as expected for a bounded linear flow system.

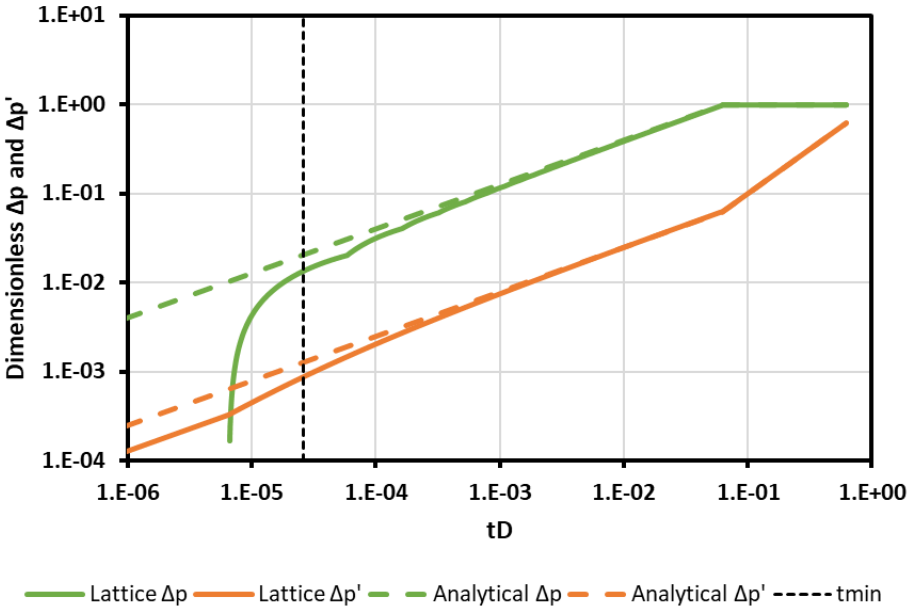

Fig. 18 – Diagnostic Plot for the Synthetic Pore Network

3.2 Sandstone Pore Network Model Results

The comparison of the PSS permeability results with the previous methods in **Table 9** shows the PSS results match the lab results relatively well, but has a big difference compared to the OpenFOAM result. The steady state result is calculated from reference nodes to outlet nodes using the reference length of the sample and best matches the PSS results.

Direction	Permeability (Darcy)				
	Lab	OpenFOAM	Steady State	Diffuse Source PSS	
X	3.0	2.6	3.4	X1: 3.1 X2: 3.7	Harmonic Average 3.36
Y			3.5	Y1: 3.5 Y2: 3.5	Harmonic Average 3.48
Z			3.6	Z1: 3.7 Z2: 3.3	Harmonic Average 3.51

Table 9 – Permeability Comparison Between Different Methods for the Sandstone Model

Looking at the drainage volume variation with time in the X direction, we see that the lattice result shows the pore network drains slower than it would have for a completely homogeneous sample (**Fig. 19**). The difference between the analytical and lattice drainage volume fraction is relatively small and the shape of the curves are very similar, which indicate that the sandstone pore network is relatively homogeneous.

The transmissibility of the lattice and analytical solutions are relatively similar, especially for the X2 face (**Fig. 20**). The transmissibility of the other methods are calculated using Eq.23 and the reference length of the sample. The transmissibility of other methods matches best with the DS transmissibility at 100% drainage volume as expected. The difference of transmissibility between the two faces indicate there is anisotropy due to flow direction.

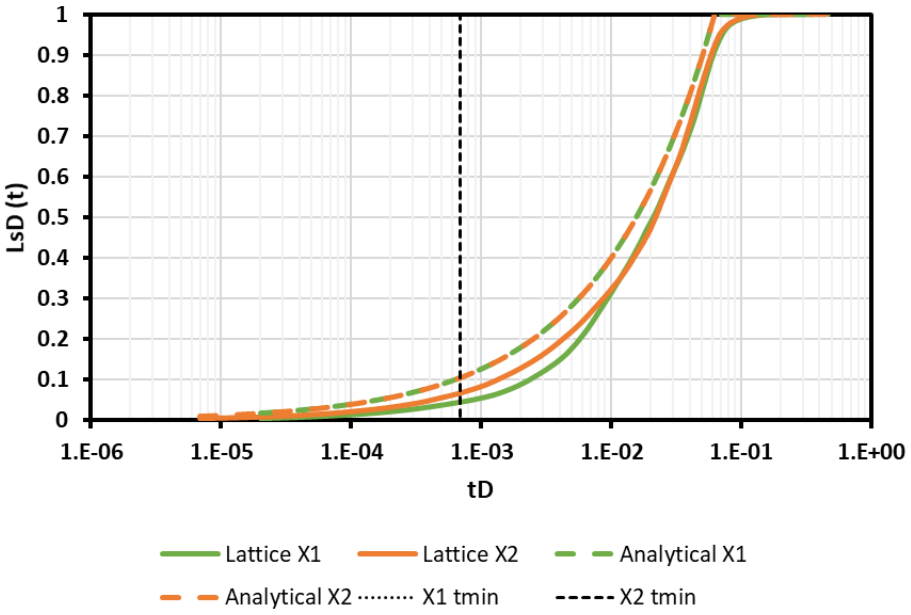

Fig. 19 – LsD Comparison Between Lattice and Analytical for the Two Faces in the X Direction of the Sandstone Pore Network

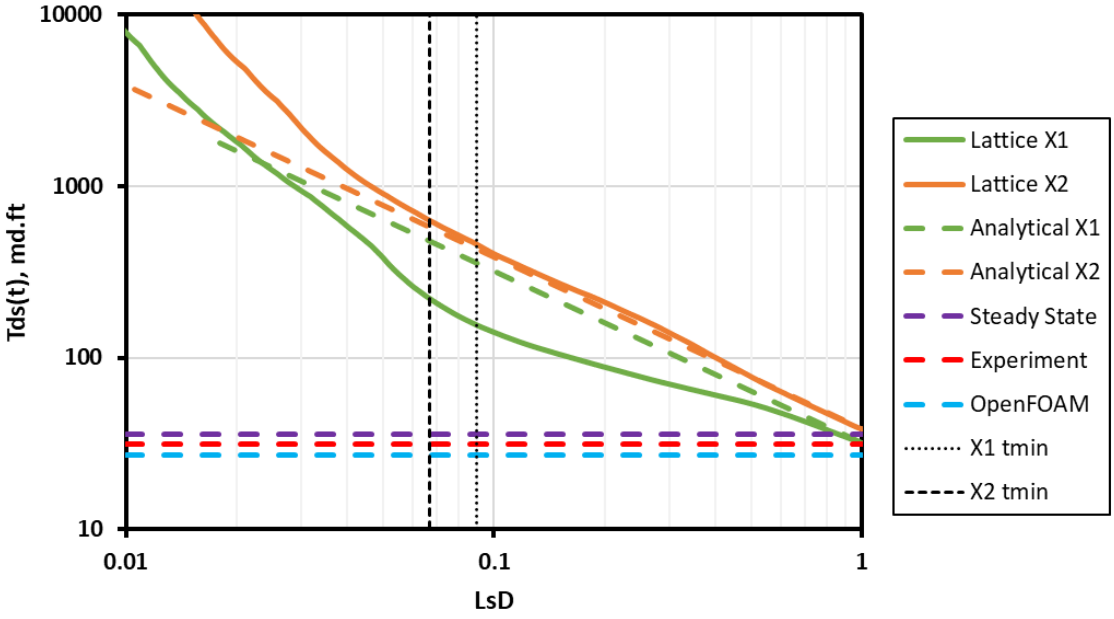

Fig. 20 – Transmissibility Comparison for the Two Faces in the X Direction of the Sandstone Pore Network

Since the sandstone pore network is relatively homogeneous, we are able to use Eq.23 to find the effective permeability. The permeability of X2 face during the transient period is slightly higher than the PSS permeability, while the permeability of X1 face is lower (**Fig. 21**).

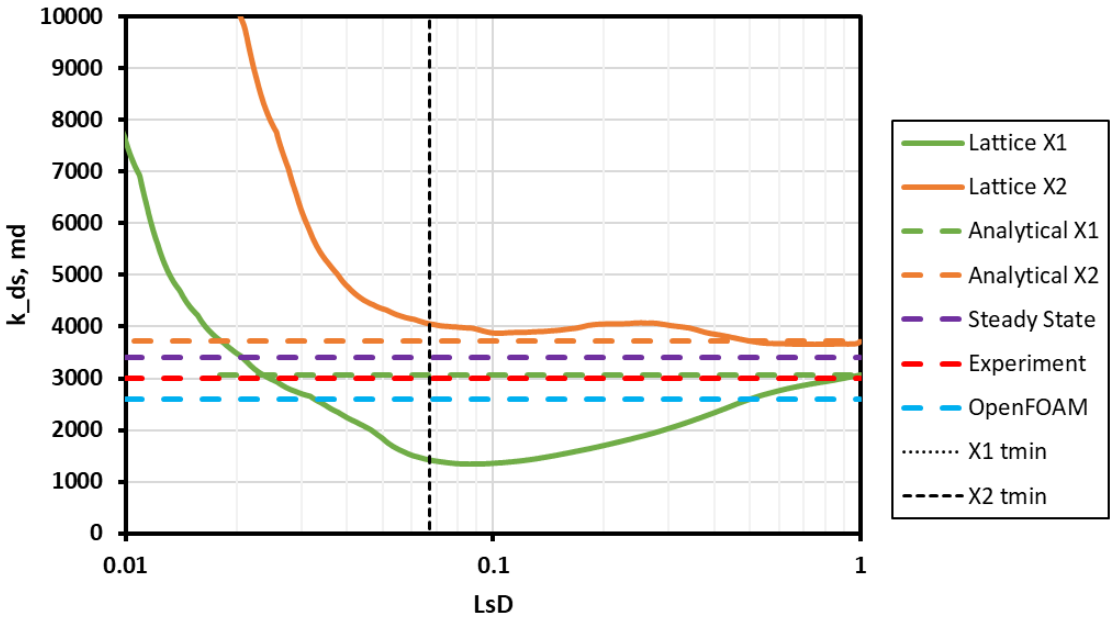

Fig. 21 – Permeability Comparison for the Two Faces in the X Direction of the Sandstone Pore Network

Looking at the diagnostic plots for the X direction, we see that the X1 face did not have linear flow until later in time and eventually become PSS flow (**Fig. 22**). The X2 face diagnostic plot shows a near perfect linear flow transitioning into PSS flow (**Fig. 23**).

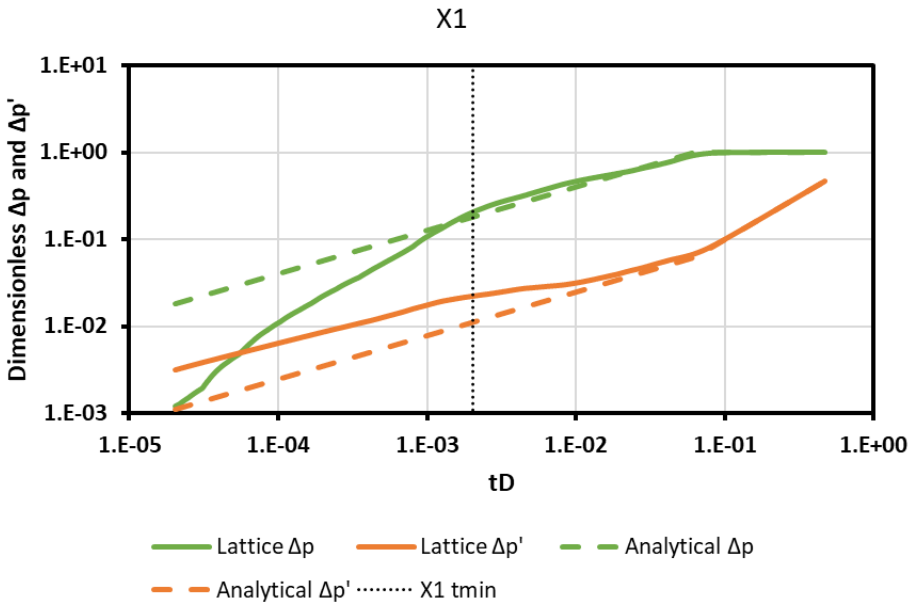

Fig. 22 – Diagnostic Plot for the X1 Face of the Sandstone Pore Network

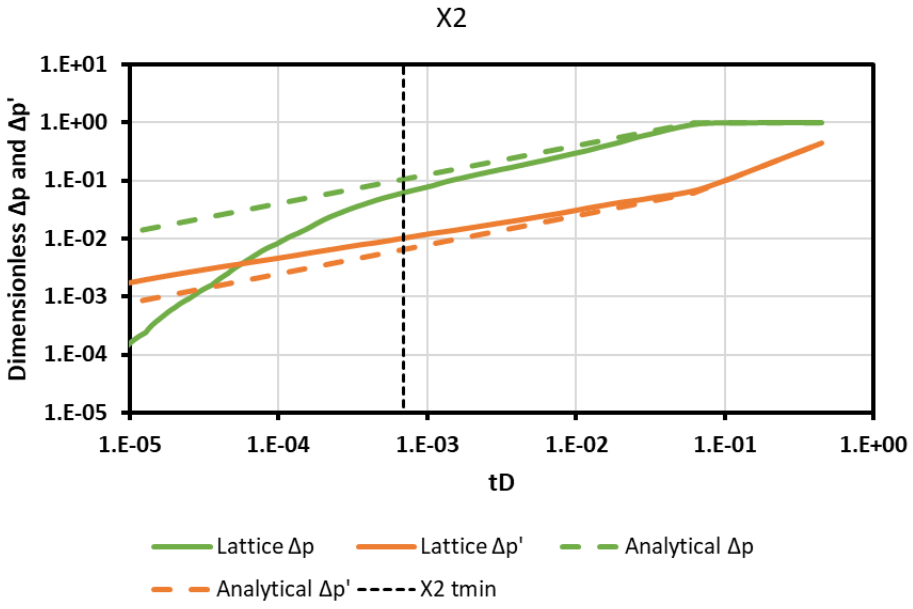

Fig. 23 – Diagnostic Plot for the X2 Face of the Sandstone Pore Network

We can actually see the drainage pattern of the pore network as shown in **Fig. 24**. To improve the visualization of the spatial patterns, the point node form of the source term is used in this display. At 10% drainage volume fraction, only the nodes at the outflowing face are drained. When the drainage volume fraction increased to 50%, the drainage pattern showed uniform drainage to the center of the sample. At high drainage volume, the uniform drainage has reached the reference face.

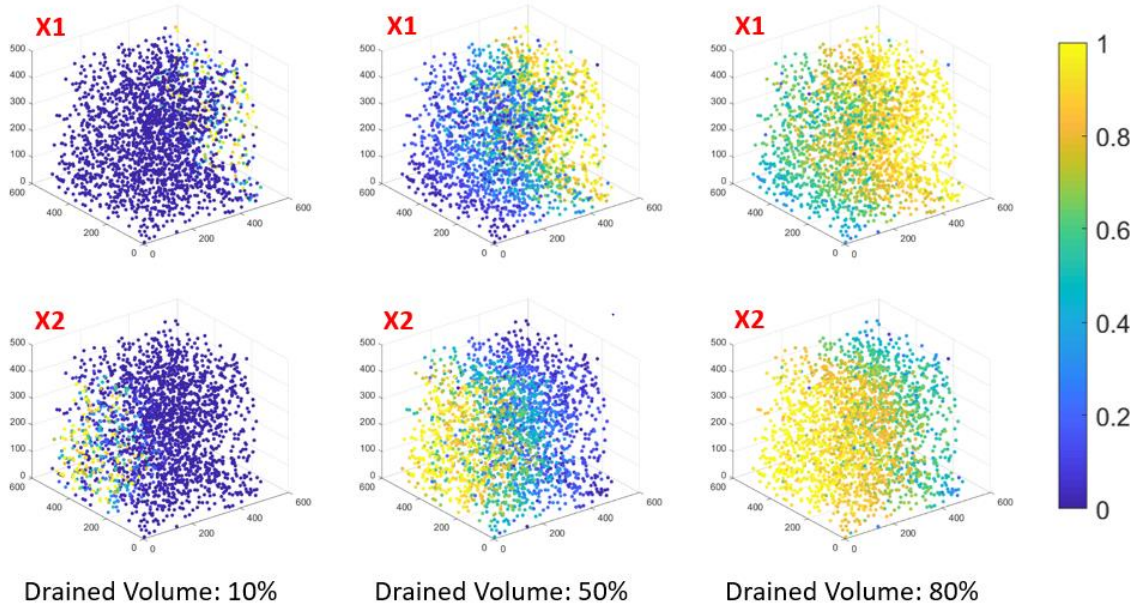

Fig. 24 – Drainage Patterns for the Two Faces in the X Direction of the Sandstone Pore Network (Liu and King, 2019). Reprinted with permission of Society of Petroleum Engineers.

3.3 Carbonate Pore Network Model Results

The result comparison for the carbonate pore network model are shown in **Table 10**. The difference between the two steady state methods is the SSF method assumes flow from face to face and utilize the sample length for its calculation, while the SS method assumes flow from reference nodes to outlet nodes and utilize the reference length for its

calculation. The PSS results are higher than the SSF and lower than the SS results. It matches relatively well with the WTD results, but has a large difference compared to the DOI method.

Direction	Permeability (md)					
	SSF	Well Test Derivative	Depth of Investigation	SS	Diffuse Source PSS	
X	1,367	1,800	34,300	1,459	X1: 1,140 X2: 1,795	Harmonic Average 1,394
Y	1,682	1,300	37,200	1,874	Y1: 1,812 Y2: 1,693	Harmonic Average 1,750
Z	1,219	1,700	36,200	1,331	Z1: 1,242 Z2: 1,331	Harmonic Average 1,285

Table 10 – Permeability Comparison Between Different Methods for the Carbonate Pore Network

The comparison of the drainage volume fraction between the lattice and analytical shows there exist a higher level of heterogeneity for the carbonate than the sandstone pore network (**Fig. 25**). The level of internal heterogeneity is especially high for the X1 face as shown by the huge deviation from the analytical curves.

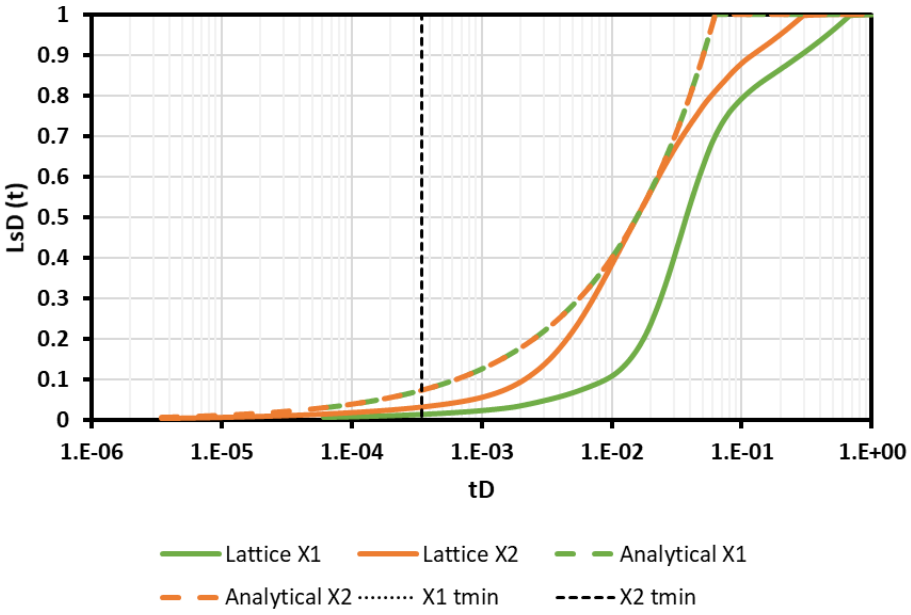

Fig. 25 – LsD Comparison Between Lattice and Analytical for the Two Faces in the X Direction of the Carbonate Pore Network

The comparison of transmissibility indicate that all methods utilize the entire pore network for their permeability calculations with the exception of DOI method. As shown in **Fig. 26**, the DOI transmissibility is extremely high, corresponding to the transient diffuse source transmissibility calculated with a very small amount of pore volume. This is expected, since the DOI method measures the permeability of the most permeable pathway between across the sample. Again, the transmissibility difference between the two faces indicate anisotropy due to the direction of flow. We cannot use the lattice equations to calculate transient permeability due to the high degree of internal heterogeneity.

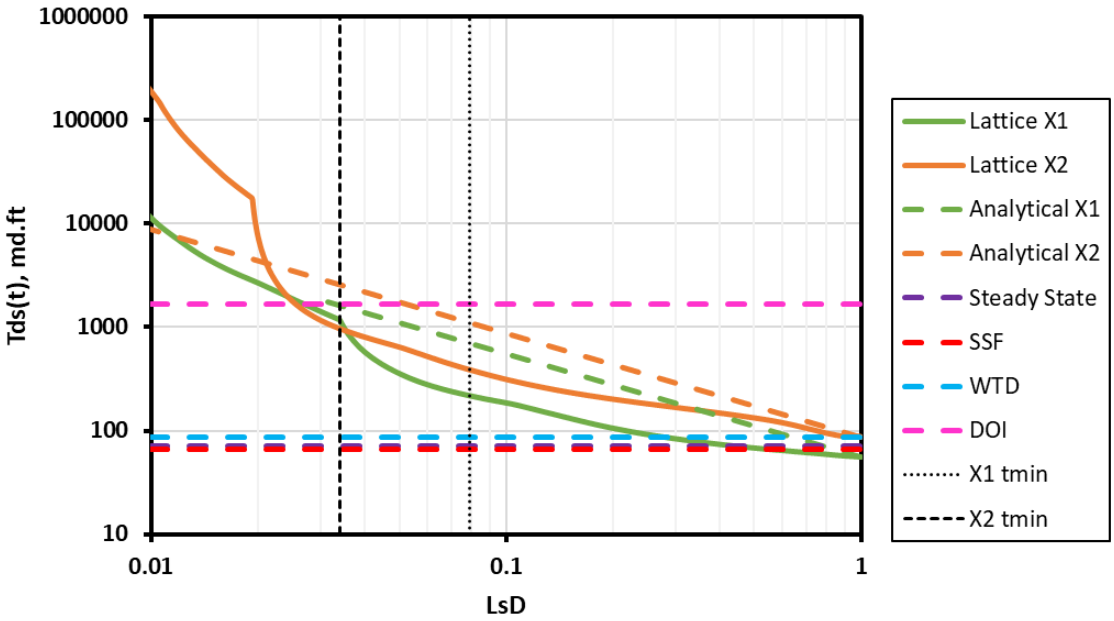

Fig. 26 – Transmissibility Comparison for the Two Faces in the X Direction of the Carbonate Pore Network

Looking at the diagnostic plot of the X1 face, we see that linear flow ended at very early time (**Fig. 27**). For the X2 face, linear flow seemed to have lasted a little longer, but also soon transitioned into a non-identifiable flow regime before reaching PSS flow (**Fig. 28**).

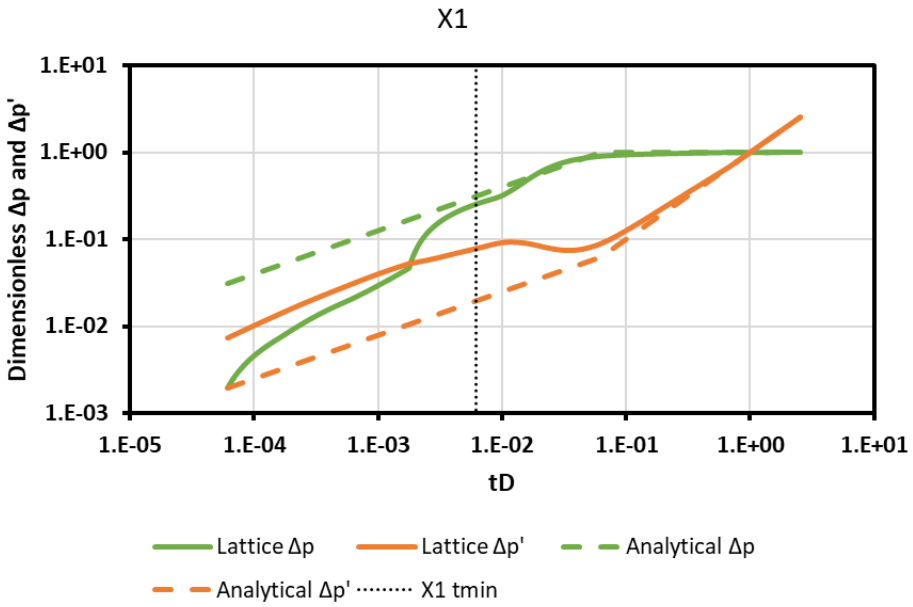

Fig. 27 – Diagnostic Plot for the X1 Face of the Carbonate Pore Network

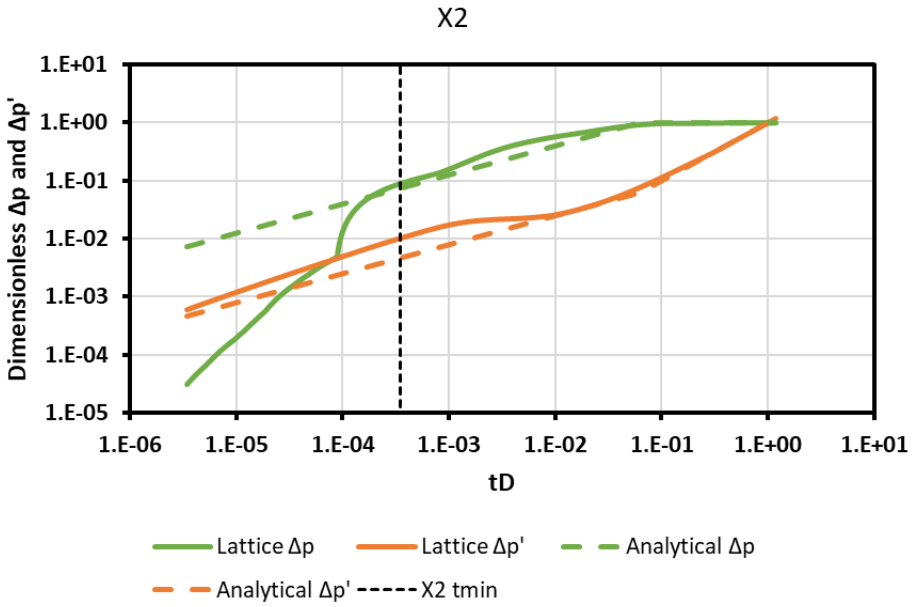

Fig. 28 – Diagnostic Plot for the X2 Face of the Carbonate Pore Network

The drainage pattern for the carbonate pore network can be visualized in **Fig. 29**. When the drainage volume was only 30% of the total pore volume, only the nodes close to the outlet face are heavily drained. As the total volume drained increased to 70%, we see the high permeable pathways within the pore network represented by the yellow streaks. Finally, when the total drainage volume reached 90%, we can see the low permeability volumes indicated by the green color. Notice the volumes of low permeability are different for the two opposite faces.

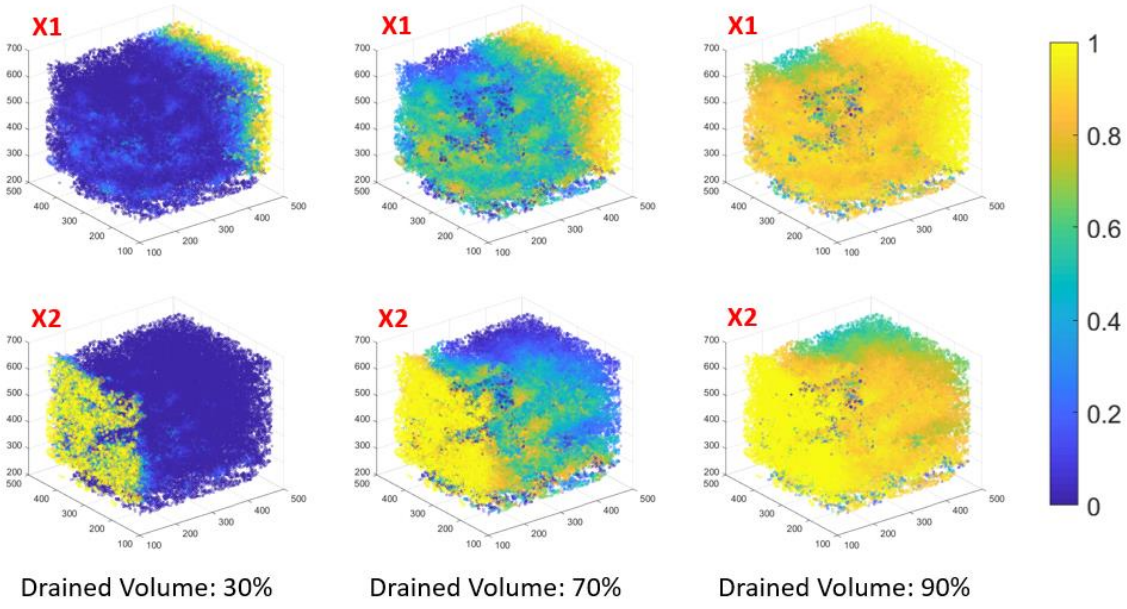

Fig. 29 – Drainage Patterns for the Two Faces in the X Direction of the Carbonate Pore Network (Liu and King, 2019). Reprinted with permission of Society of Petroleum Engineers.

3.5 Conclusions and Recommendations for Future Work

The diffuse source methodology has been applied to both the carbonate and the sandstone pore networks. The results from these two pore networks led us to make the following conclusions:

1. The DS method can calculate the effective transmissibility of the pore network during the transient to PSS flow periods
2. The DS effective permeability can be calculated for pore networks that are relatively homogeneous
3. The diffuse source PSS results compare very well with the results of steady state, WTD and lab measurements
4. The permeability of DOI method is a transient permeability that measures the most permeable sub volume across the pore network indicated by the DS results
5. The DS method lets us visualize the sub volume that contributes to the effective transmissibility calculation from transient to PSS flow
6. The comparison between the analytical and lattice solutions for the DS method can indicate the degree of heterogeneity within the pore network
7. The comparison of drainage volume fraction and effective transmissibility when two opposing faces are chosen as the flowing face can indicate the level of anisotropy due to direction of flow

Since the advantage of the diffuse source method is its capability to capture transmissibility and sometimes permeability during the transient flow regime, it might be especially useful for unconventional pore networks. My recommendation for next step forward is to apply the DS method to an unconventional pore network. Also, it would be very useful to find a method to convert the DS transmissibility to permeability during the transient flow period for pore networks that are internally highly heterogeneous.

REFERENCES

Bakke, S. and Øren, P.-E. 1997. 3-D Pore-Scale Modelling of Sandstones and Flow Simulations in the Pore Networks. *SPE Journal* **2** (02): 136-149. DOI: 10.2118/35479-PA

Blunt, M.J., Jackson, M.D., Piri, M. et al. 2002. Detailed Physics, Predictive Capabilities and Macroscopic Consequences for Pore-Network Models of Multiphase Flow. *Advances in Water Resources* **25** (8): 1069-1089.

Bourbie, T. and Walls, J. 1982. Pulse Decay Permeability: Analytical Solution and Experimental Test. *Society of Petroleum Engineers Journal* **22** (05): 719-721. DOI: 10.2118/9744-PA

Brace, W.F., Walsh, J.B., and Frangos, W.T. 1968. Permeability of Granite under High Pressure. **73** (6): 2225-2236. DOI: doi:10.1029/JB073i006p02225

Choquette, P. and Pray, L. 1970. *Geologic Nomenclature and Classification of Porosity in Sedimentary Carbonates* Original edition. ISBN.

Coles, M.E., Hazlett, R.D., Spanne, P. et al. 1998. Pore Level Imaging of Fluid Transport Using Synchrotron X-Ray Microtomography. *Journal of Petroleum Science and Engineering* **19** (1): 55-63. DOI: https://doi.org/10.1016/S0920-4105(97)00035-1

Coles, M.E., Muegge, E.L., Spanne, P. et al. 1995. *Computed Microtomography of Reservoir Core Samples*. Conference: 1994 International Symposium of the Society of Core Analysts, Stavanger (Norway), 12-14 Sep 1994; Other Information: Pbd: [1995]: ; Brookhaven National Lab., Upton, NY (United States). Original edition. ISBN BNL-60656; CONF-9409305-1; Other: ON: DE95008384;

TRN: 95:003053 United States Other: ON: DE95008384; TRN: 95:003053 OSTI as DE95008384 BNL English.

Cormen, T.H., Leiserson, C.E., Rivest, R.L. et al. 2009. *Introduction to Algorithms*: Massachusetts Institute of Technology. Original edition. ISBN 9780262533058.

Dijkstra, E.W. 1959. A Note on Two Problems in Connexion with Graphs. *Numerische Mathematik* **1** (1): 269-271. DOI: 10.1007/BF01386390

Dunham, R.J. 1962. Classification of Carbonate Rocks According to Depositional Texture1. In *Classification of Carbonate Rocks—a Symposium*, ed. Ham, W.E.: American Association of Petroleum Geologists.

Dunsmuir, J.H., Ferguson, S.R., D'Amico, K.L. et al. 1991. X-Ray Microtomography: A New Tool for the Characterization of Porous Media. Paper presented at the SPE Annual Technical Conference and Exhibition, Dallas, Texas. 8. Society of Petroleum Engineers. DOI: 10.2118/22860-MS.

Ehrenberg, S.N. and Nadeau, P.H. 2005. Sandstone Vs. Carbonate Petroleum Reservoirs: A Global Perspective on Porosity-Depth and Porosity-Permeability Relationships. *AAPG Bulletin* **89** (4): 435-445. DOI: 10.1306/11230404071

Fatt, I. 1956. The Network Model of Porous Media. In:38: Society of Petroleum Engineers.

Flannery, B.P., Deckman, H.W., Roberge, W.G. et al. 1987. Three-Dimensional X-Ray Microtomography. *Science* **237** (4821): 1439-1444. DOI: 10.1126/science.237.4821.1439

Gupta, A. and Poppelreiter, M. 2010. Innovative Field Camp for Education and Industry-Academic Collaboration in Geology-Based Reservoir Model Building for Carbonate Reservoirs in the Middle East. Paper presented at the SPE Annual Technical Conference and Exhibition, Florence, Italy. 10. Society of Petroleum Engineers. DOI: 10.2118/134453-MS.

Hsieh, P.A., Tracy, J.V., Neuzil, C.E. et al. 1981. A Transient Laboratory Method for Determining the Hydraulic Properties of 'Tight' Rocks—I. Theory. *International Journal of Rock Mechanics and Mining Sciences & Geomechanics Abstracts* **18** (3): 245-252. DOI: https://doi.org/10.1016/0148-9062(81)90979-7

James, N.P. and Jones, B. 2015. *Origin of Carbonate Sedimentary Rocks*: Wiley. Original edition. ISBN 9781118652701.

King, M.J., Wang, Z., and Datta-Gupta, A. 2016. Asymptotic Solutions of the Diffusivity Equation and Their Applications. Paper presented at the SPE Europec featured at 78th EAGE Conference and Exhibition, Vienna, Austria. 37. Society of Petroleum Engineers. DOI: 10.2118/180149-MS.

Kulkarni, K.N., Datta-Gupta, A., and Vasco, D.W. 2001. A Streamline Approach for Integrating Transient Pressure Data into High-Resolution Reservoir Models. *SPE Journal* **6** (03): 273-282. DOI: 10.2118/74135-PA

Kumar, M. 2009. Multiphase Flow in Reservoir Cores Using Digital Core AnalysisPh.D., Australian National University.

Lee, J. 1982. *Well Testing*: New York: Society of Petroleum Engineers. Original edition. ISBN 0895203170.

Li, C.K., Michael J. 2016. Integration of Pressure Transient Data into Reservoir Models Using the Fast Marching Method, Spe-180148-Ms. In *SPE Europec featured at 78th EAGE Conference and Exhibition*. Vienna, Austria: Society of Petroleum Engineers.

Li, H. 2016. Wave Propagation Models Capture Pressure Behavior in Heterogeneous Unconventional Reservoirs. Paper presented at the SPE Annual Technical Conference and Exhibition, Dubai, UAE. 13. Society of Petroleum Engineers. DOI: 10.2118/184504-STU.

Lindquist, W.B., Lee, S.-M., Coker, D.A. et al. 1996. Medial Axis Analysis of Void Structure in Three-Dimensional Tomographic Images of Porous Media. *Journal of Geophysical Research: Solid Earth* **101** (B4): 8297-8310. DOI: 10.1029/95JB03039

Liu, C.-H., Nunna, K., Syed, I. et al. 2019. Evaluation of Upscaling Approaches for the Amellago Carbonate Outcrop Model, Spe-195560-Ms. Paper presented at the SPE Europec featured at the 81st EAGE Conference and Exhibition, London, England. Society of Petroleum Engineers.

Liu, S. and King, M.J. 2019. Improved Calculation of Effective Permeability for Pore Network Models Using the Diffuse Source Methodology, Spe-195539-Ms. Paper presented at the SPE Europec featured at the 81st EAGE Conference and Exhibition, London, England. Society of Petroleum Engineers.

MacDonald, R.M., Kersey, D.G., Zhang, T. et al. 2009. Effect of Carbonate Heterogeneity on Core - Log Integration. Paper presented at the Kuwait International Petroleum

Conference and Exhibition, Kuwait City, Kuwait. 15. Society of Petroleum Engineers. DOI: 10.2118/127290-MS.

Malone, A., King, M.J., and Wang, Z. 2019. Characterization of Multiple Transverse Fracture Wells Using the Asymptotic Approximation of the Diffusivity Equation, Spe-195505-Ms. Paper presented at the SPE Europec featured at the 81st EAGE Conference and Exhibition, London, England. Society of Petroleum Engineers.

Mani, V. and Mohanty, K.K. 1998. Pore-Level Network Modeling of Three-Phase Capillary Pressure and Relative Permeability Curves. *SPE Journal* **3** (03): 238-248. DOI: 10.2118/50942-PA

Manwart, C.A., U.;Koponen, A.;Hilfer, R.;Timonen, J. 2002. Lattice-Boltzmann and Finite-Difference Simulations for the Permeability for Three-Dimensional Porous Media. *Phys Rev E* **66**: 16702-16713.

Mirabolghasemi, M., Prodanović, M., Dicarlo, D. et al. 2015. Prediction of Empirical Properties Using Direct Pore-Scale Simulation of Straining through 3d Microtomography Images of Porous Media. *Journal of Hydrology* **529**: 768-778. DOI: 10.1016/j.jhydrol.2015.08.016

Ning, X., Fan, J., Holditch, S.A. et al. 1993. The Measurement of Matrix and Fracture Properties in Naturally Fractured Cores. Paper presented at the Low Permeability Reservoirs Symposium, Denver, Colorado. 15. Society of Petroleum Engineers. DOI: 10.2118/25898-MS.

Nunna, K. and King, M.J. 2017. Dynamic Downscaling and Upscaling in High Contrast Systems. Paper presented at the SPE Reservoir Simulation Conference,

Montgomery, Texas, USA. 26. Society of Petroleum Engineers. DOI: 10.2118/182689-MS.

Oren, P.E., Bakke, S., and Arntzen, O.J. 1998. Extending Predictive Capabilities to Network Models. *SPE Journal* **3** (04): 324-336. DOI: 10.2118/52052-PA

Pasumarti, A. 2014. Exploring an Unstructured Lattice Representation for Carbonate Reservoir CharacterizationMaster's Thesis, Texas A&M University.

Pasumarti, A., Sengupta, S., and Michael, J.K. 2015. A Novel Transient Simulation Based Methodology for the Calculation of Permeability in Pore Network Models. Paper presented at the Abu Dhabi International Petroleum Exhibition and Conference, Abu Dhabi, UAE. 28. Society of Petroleum Engineers. DOI: 10.2118/177884-MS.

Patzek, T.W. 2001. Verification of a Complete Pore Network Simulator of Drainage and Imbibition. *SPE Journal* **6** (02): 144-156. DOI: 10.2118/71310-PA

Saadi, F.A., Wolf, K.-H., and Kruijsdijk, C.v. 2017. Characterization of Fontainebleau Sandstone: Quartz Overgrowth and Its Impact on Pore-Throat Framework. *Journal of Petroleum & Environmental Biotechnology* **8** (3). DOI: 10.4172/2157-7463.1000328

Scholle, P.A., Bebout, D.G., and Moore, C.H. 1983. *Carbonate Depositional Environments* Original edition. ISBN.

Sengupta, S. 2016. Determination of Permeability from Pore Network Models by Using a Novel Transient Simulation MethodologyMaster's Thesis, Texas A&M University.

Vasco, D.W. and Datta-Gupta, A. 1999. Asymptotic Solutions for Solute Transport: A Formalism for Tracer Tomography. *WATER RESOURCES RESEARCH* **35** (1): 1-16. DOI: doi:10.1029/98WR02742

Virieux, J., Flores‐Luna, C., and Gibert, D. 1994. Asymptotic Theory for Diffusive Electromagnetic Imaging. *Geophysical Journal International* **119** (3): 857-868. DOI: 10.1029/98WR02742

Wang, S.Y., Ayral, S., Castellana, F.S. et al. 1984. Reconstruction of Oil Saturation Distribution Histories During Immiscible Liquid-Liquid Displacement by Computer-Assisted Tomography. *AIChE Journal* **30** (4): 642-646. DOI: 10.1002/aic.690300418

Wang, Z., Li, C., and King, M. 2017. Validation and Extension of Asymptotic Solutions of Diffusivity Equation and Their Applications to Synthetic Cases. Paper presented at the SPE Reservoir Simulation Conference, Montgomery, Texas, USA. Society of Petroleum Engineers. DOI: 10.2118/182716-MS.

Wellington, S.L. and Vinegar, H.J. 1987. X-Ray Computerized Tomography. *Journal of Petroleum Technology* **39** (08): 885-898. DOI: 10.2118/16983-PA

Xu, B., Kamath, J., Yortsos, Y.C. et al. 1999. Use of Pore-Network Models to Simulate Laboratory Corefloods in a Heterogeneous Carbonate Sample. *SPE Journal* **4** (03): 178-186. DOI: 10.2118/57664-PA

Yang, C., Sharma, V.K., Datta-Gupta, A. et al. 2015. A Novel Approach for Production Transient Analysis of Shale Gas/Oil Reservoirs. Paper presented at the Unconventional Resources Technology Conference, San Antonio, Texas, USA.

22. Unconventional Resources Technology Conference. DOI: 10.15530/URTEC-2015-2176280.

Youssef, S., Rosenberg, E., Gland, N.F. et al. 2007. High Resolution Ct and Pore-Network Models to Assess Petrophysical Properties of Homogeneous and Heterogeneous Carbonates. Paper presented at the SPE/EAGE Reservoir Characterization and Simulation Conference, Abu Dhabi, UAE. 12. Society of Petroleum Engineers. DOI: 10.2118/111427-MS.

APPENDIX A

ANALYTICAL EQUATIONS FOR POINT NODE REPRESENTATION

To compare with the point node lattice calculations, a set of analytical equations were derived for comparison purposes. The analytical equations are derived assuming the whole pore network has homogeneous bounded linear flow.

We assume the flow rate on the outflowing face and viscosity is constant. Therefore, transmissibility varies with the pressure drop across the pore network.

$$T_{DS} = \frac{\mu q_f}{\Delta p_{DS}} \tag{30}$$

The relationship to permeability at PSS is well-known.

$$T_{PSS} = 2kA/L \tag{31}$$

At finite times, the factor of $2/L$ is a function of time. Thus, we can first define a diffuse source flux, which can be integrated to find the pressure drop across the pore network. Diffusivity remains constant and dependent on the lattice PSS permeability due to the assumption that the entire pore network is homogeneous.

$$\hat{q}_{DS}(x,t) = \int_x^L dx e^{-x^2/4\alpha t} \Big/ \int_0^L dx e^{-x^2/4\alpha t} = 1 - erf\left(\frac{x}{\sqrt{4\alpha t}}\right) \Big/ erf\left(\frac{L}{\sqrt{4\alpha t}}\right) \tag{32}$$

$$\alpha = \frac{k}{3792\phi\mu c_t} \tag{33}$$

$$\Delta p_{DS}(t) = \frac{\mu q_f}{kA} \int_{x=0}^{L} dx\, \hat{q}(x,t) = \frac{\mu q_f}{kA} \cdot \sqrt{\frac{4\alpha t}{\pi}} \cdot \left(\frac{1 - e^{-L^2/4\alpha t}}{erf\left(L/\sqrt{4\alpha t}\right)} \right) \tag{34}$$

Transmissibility can then be computed using the pressure drop across the pore network and a dimensionless time is defined using diffusivity and sample length.

$$T_{DS}(t)=\frac{\mu q_f}{\Delta p_{DS}(t)}=kA\sqrt{\frac{\pi}{4\alpha t}}\cdot\frac{erf\left(L/\sqrt{4\alpha t}\right)}{\left(1-e^{-L^2/4\alpha t}\right)}=T_{PSS}\cdot\frac{\sqrt{\pi t_D}\cdot erf\left(1/\sqrt{4t_D}\right)}{\left(4t_D\right)\cdot\left(1-e^{-1/4t_D}\right)} \tag{35}$$

$$t_D=\frac{\alpha t}{L^2} \tag{36}$$

We can rearrange **Eq.35** to isolate permeability. We notice that α is proportional to the unknown, k, so the left hand side of **Eq.38** is approximately $\sim\sqrt{k}$, as expected for linear flow. The expression scales as $\sqrt{t}$ at early time, as expected for infinite acting linear flow and approaches a constant at large time, as expected for PSS. At large time, the product of the two expressions in **Eq.37** approaches unity, and we recover the PSS expression.

$$k=\frac{L}{2A}T_{DS}\cdot\left(\frac{2}{\sqrt{\pi}}\frac{\sqrt{4\alpha t}}{L}\right)\cdot\left(\frac{1-e^{-L^2/4\alpha t}}{erf\left(L/\sqrt{4\alpha t}\right)}\right) \tag{37}$$

$$\frac{k}{\sqrt{\alpha}}=\frac{2}{A}T_{DS}\sqrt{\frac{t}{\pi}}\cdot\left(\frac{1-e^{-L^2/4\alpha t}}{erf\left(L/\sqrt{4\alpha t}\right)}\right) \tag{38}$$

For bounded linear flow, the drainage volume has a similar time dependence and can also be calculated to compare with the lattice results.

$$V_d(t)=\left(A\phi\sqrt{\pi\alpha t}\right)\cdot erf\left(\frac{L}{\sqrt{4\alpha t}}\right)=V_p\left(\sqrt{\pi t_D}\right)erf\left(\frac{1}{2\sqrt{t_D}}\right) \tag{39}$$

APPENDIX B

SANDSTONE PORE NETWORK MODEL RESULTS

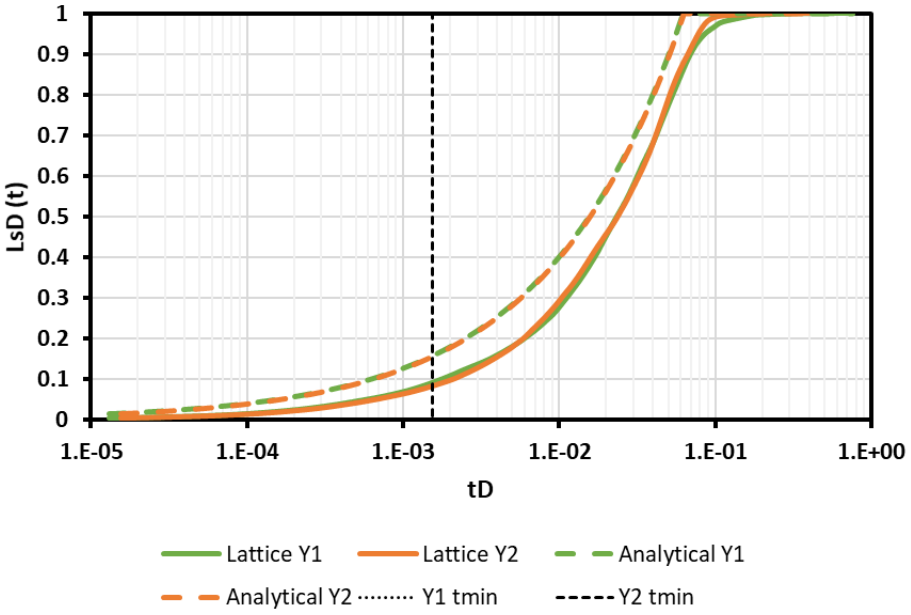

Fig. 30 – LsD Comparison Between Lattice and Analytical for the Two Faces in the Y Direction of the Sandstone Pore Network

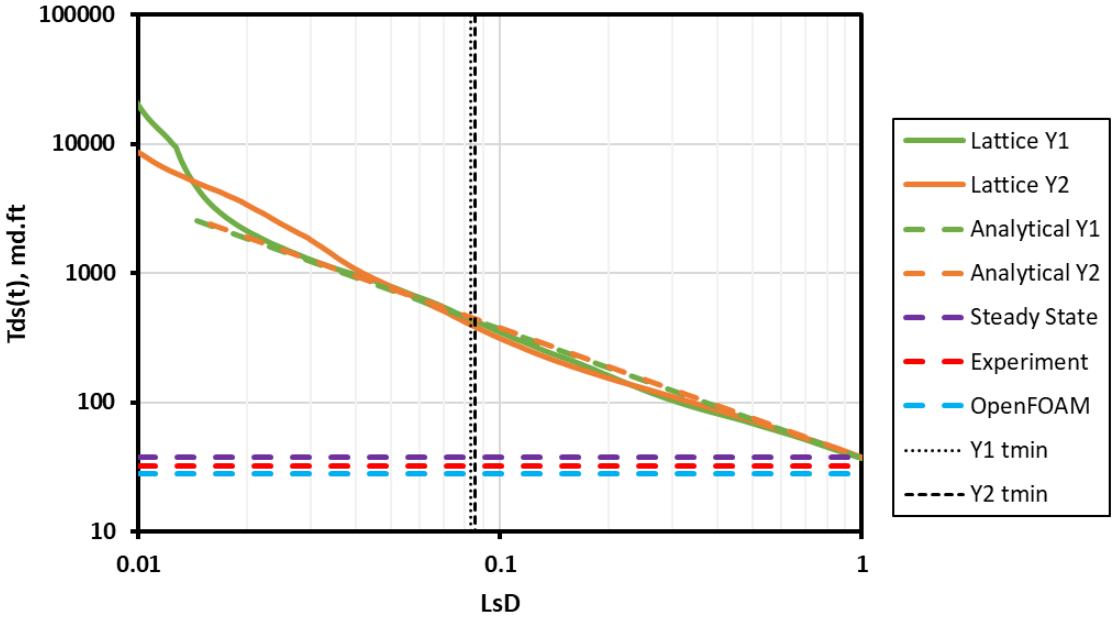

Fig. 31 – Transmissibility Comparison for the Two Faces in the Y Direction of the Sandstone Pore Network

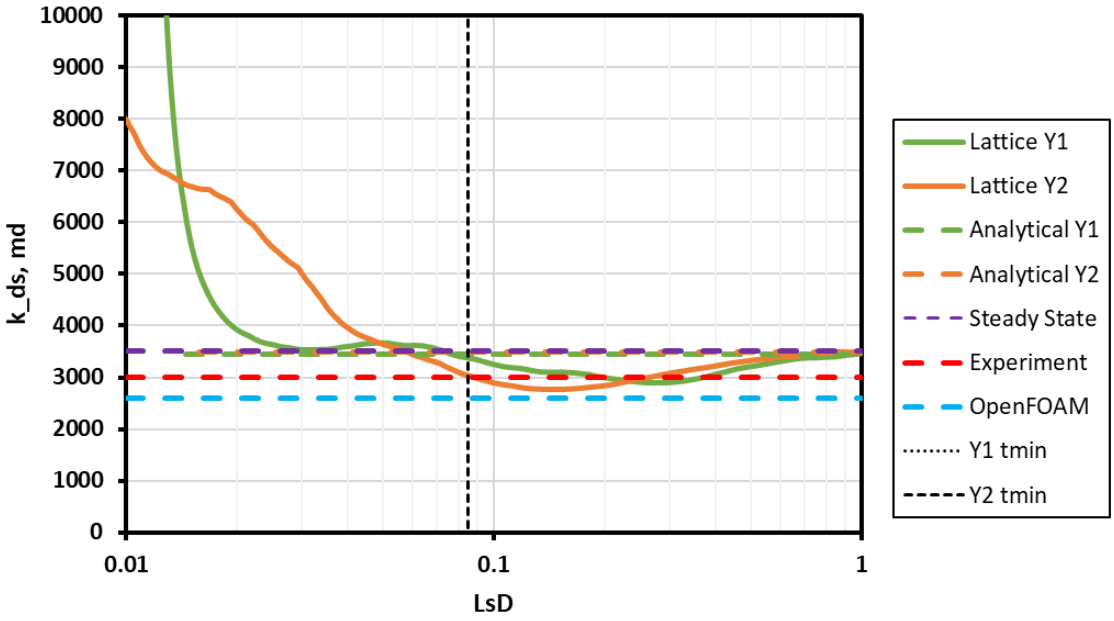

Fig. 32 – Permeability Comparison for the Two Faces in the Y Direction of the Sandstone Pore Network

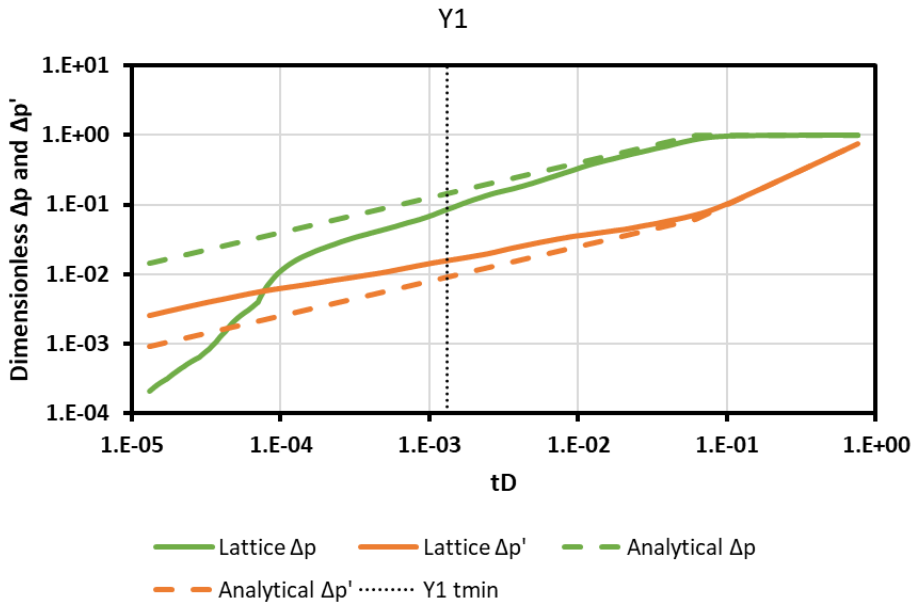

Fig. 33 – Diagnostic Plot for the Y1 Face of the Sandstone Pore Network

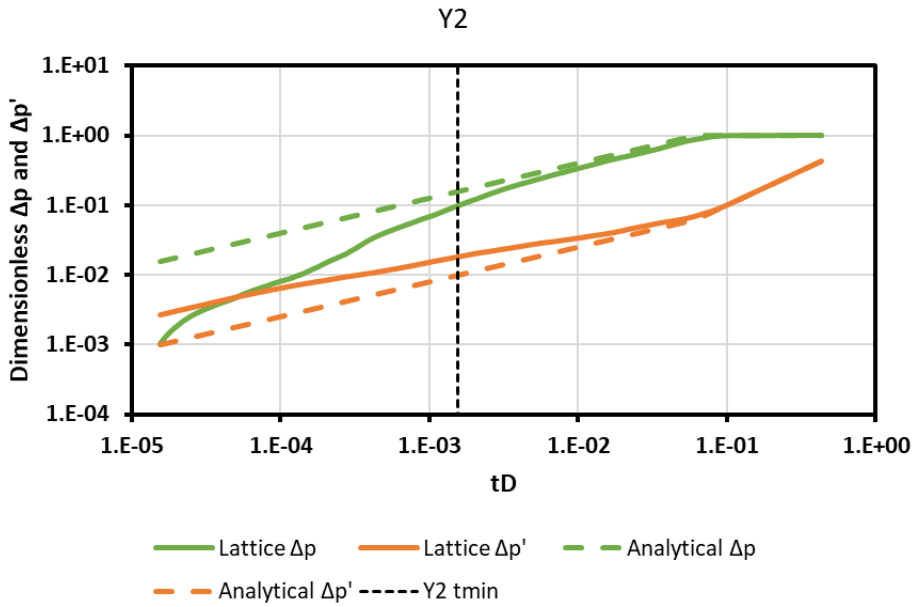

Fig. 34 – Diagnostic Plot for the Y2 Face of the Sandstone Pore Network

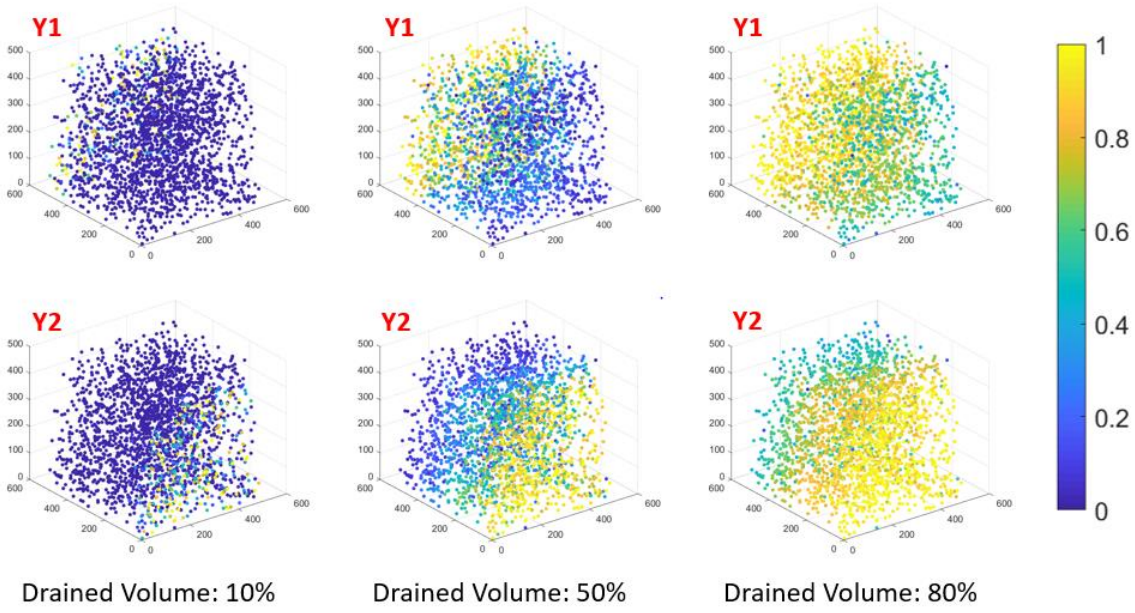

Fig. 35 – Drainage Patterns for the Two Faces in the Y Direction of the Sandstone Pore Network

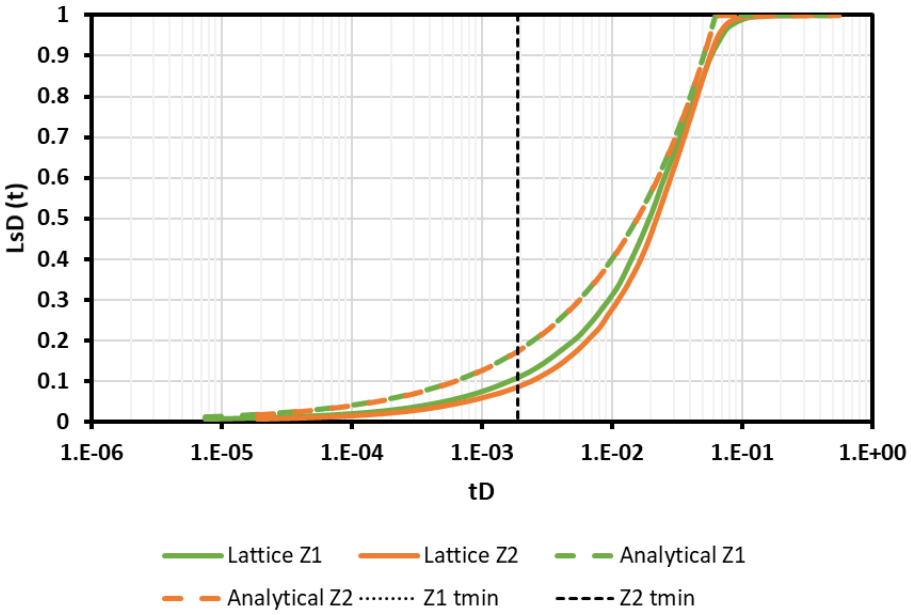

Fig. 36 – LsD Comparison Between Lattice and Analytical for the Two Faces in the Z Direction of the Sandstone Pore Network

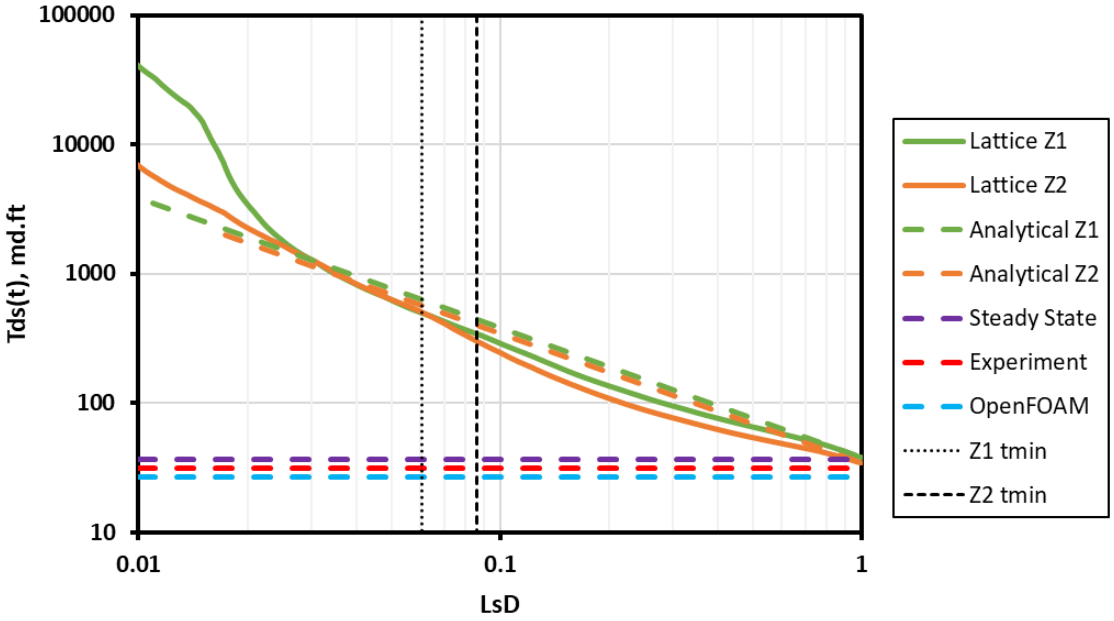

Fig. 37 – Transmissibility Comparison for the Two Faces in the Z Direction of the Sandstone Pore Network

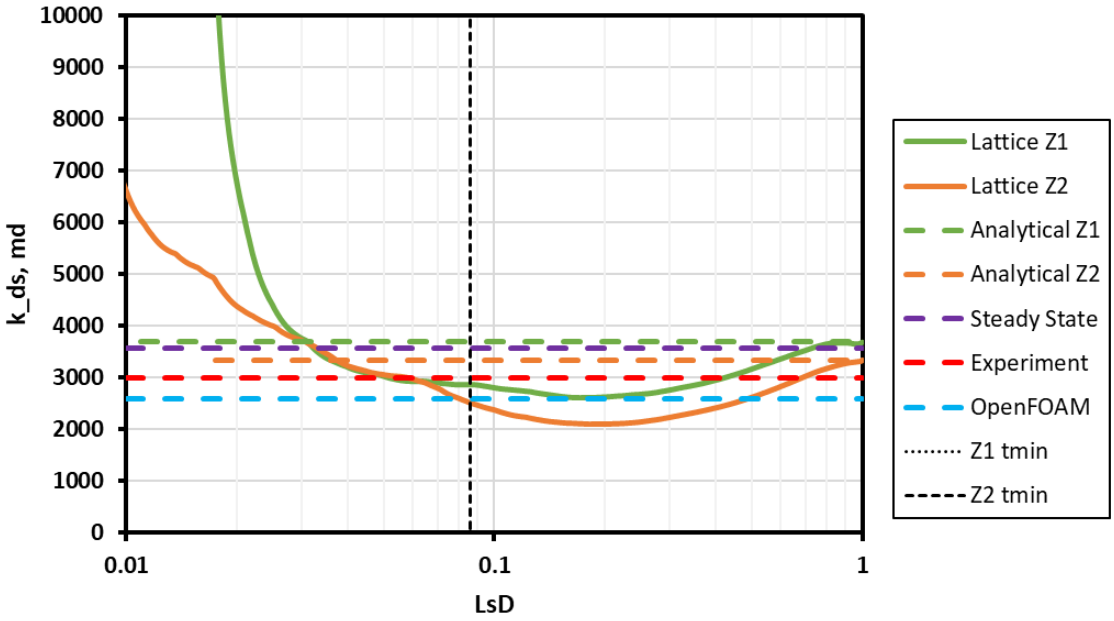

Fig. 38 – Permeability Comparison for the Two Faces in the Z Direction of the Sandstone Pore Network

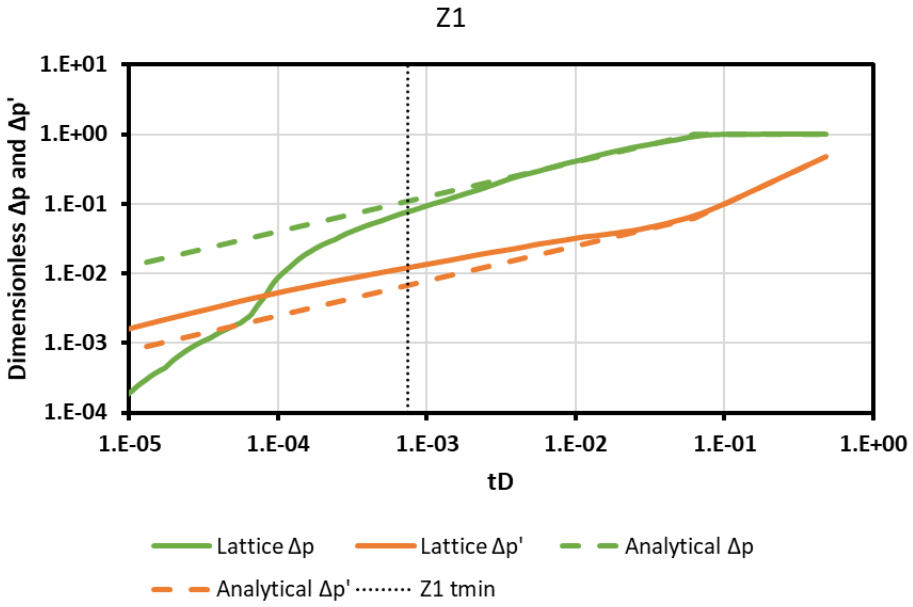

Fig. 39 – Diagnostic Plot for the Z1 Face of the Sandstone Pore Network

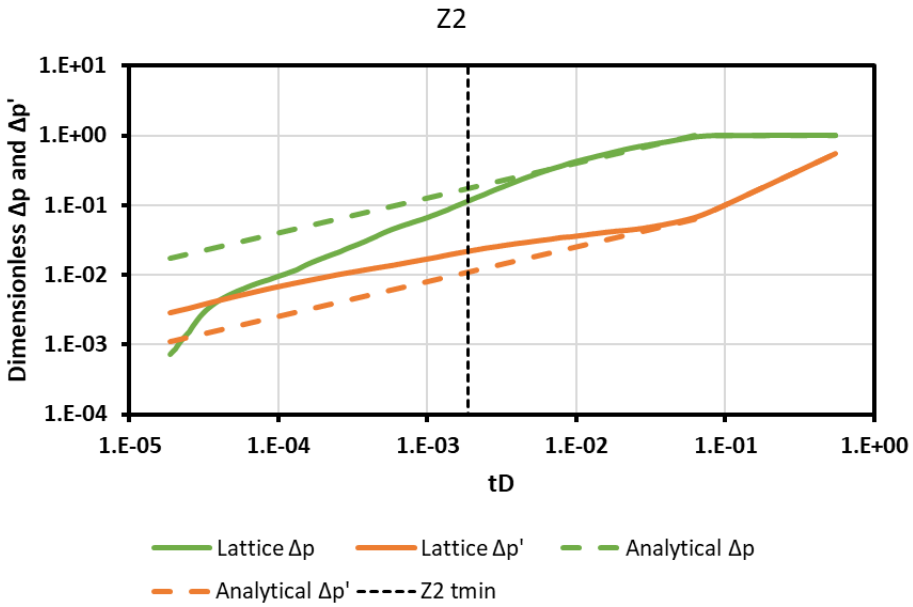

Fig. 40 – Diagnostic Plot for the Z2 Face of the Sandstone Pore Network

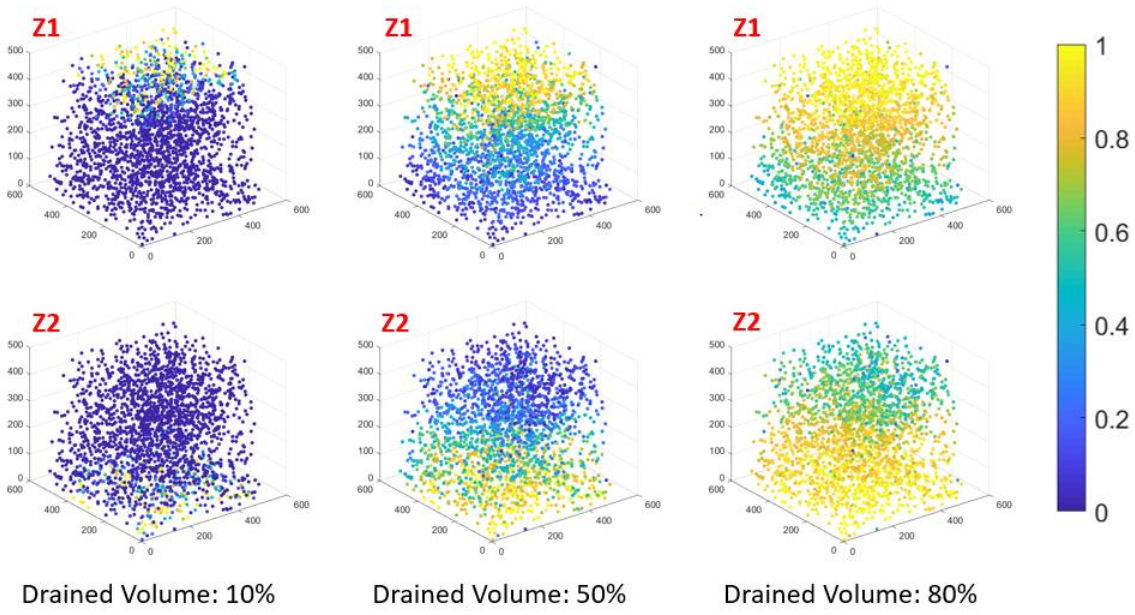

Fig. 41 – Drainage Patterns for the Two Faces in the Z Direction of the Sandstone Pore Network

APPENDIX C

CARBONATE PORE NETWORK MODEL RESULTS

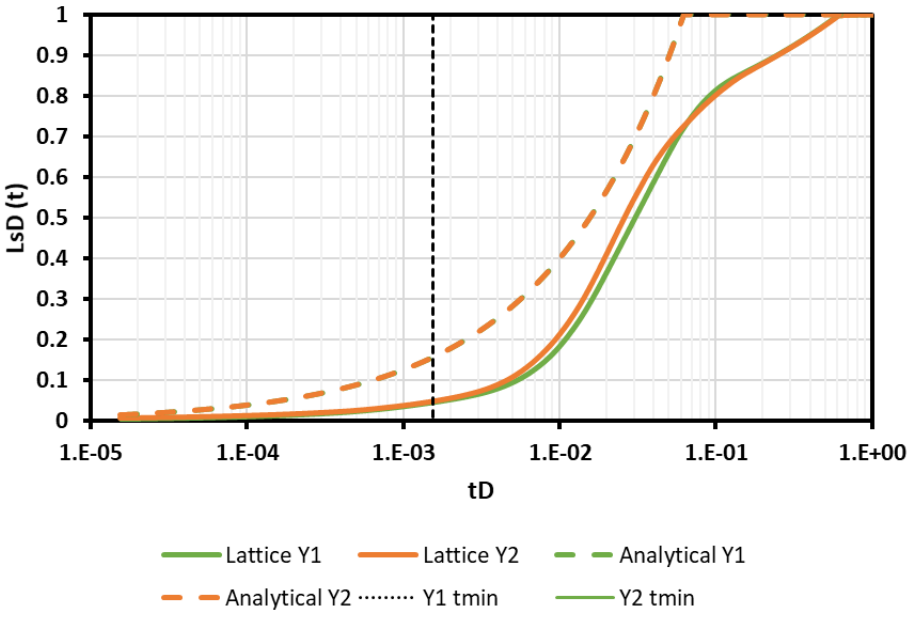

Fig. 42 – LsD Comparison Between Lattice and Analytical for the Two Faces in the Y Direction of the Carbonate Pore Network

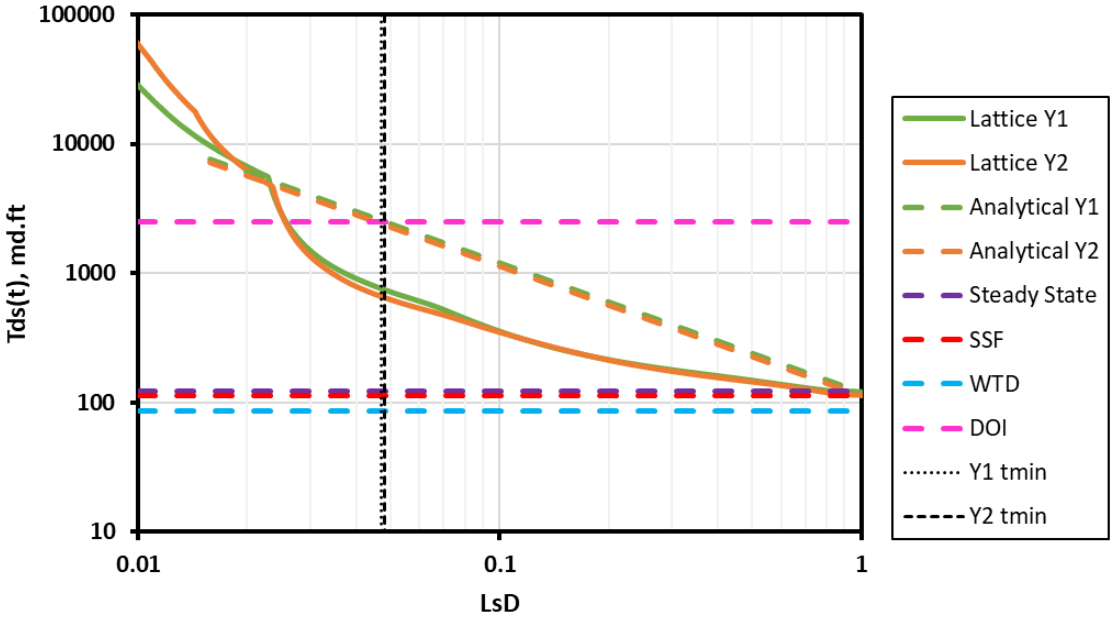

Fig. 43 – Transmissibility Comparison for the Two Faces in the Y Direction of the Carbonate Pore Network

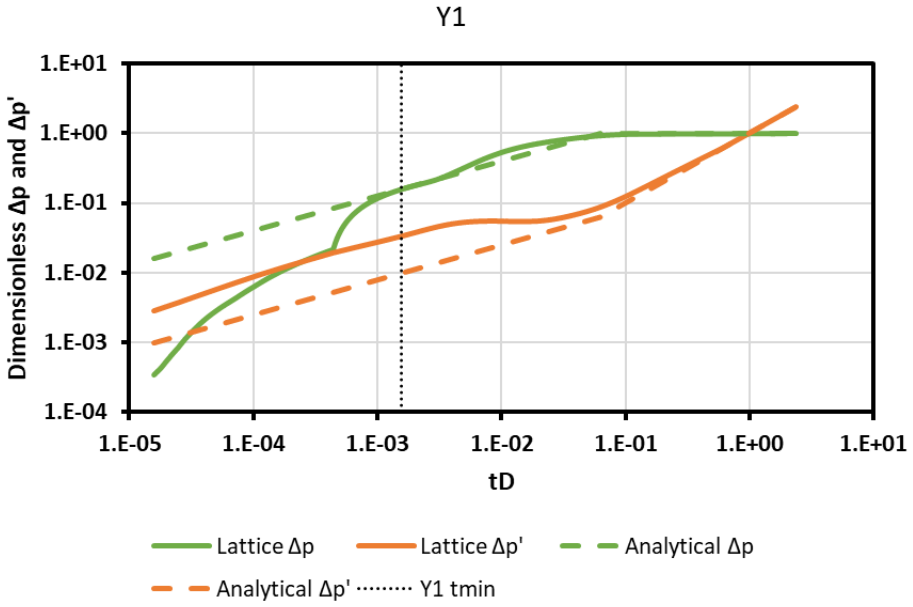

Fig. 44 – Diagnostic Plot for the Y1 Face of the Carbonate Pore Network

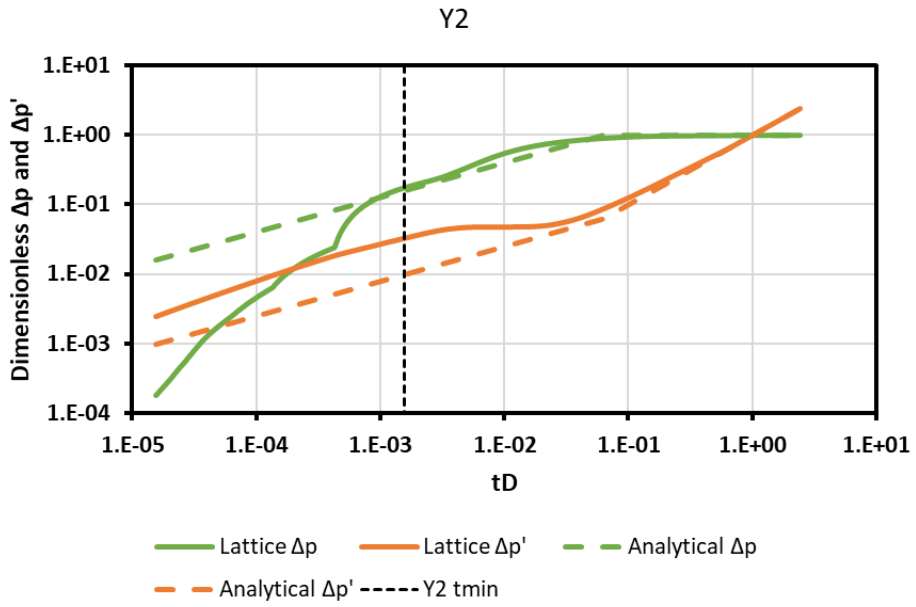

Fig. 45 – Diagnostic Plot for the Y2 Face of the Carbonate Pore Network

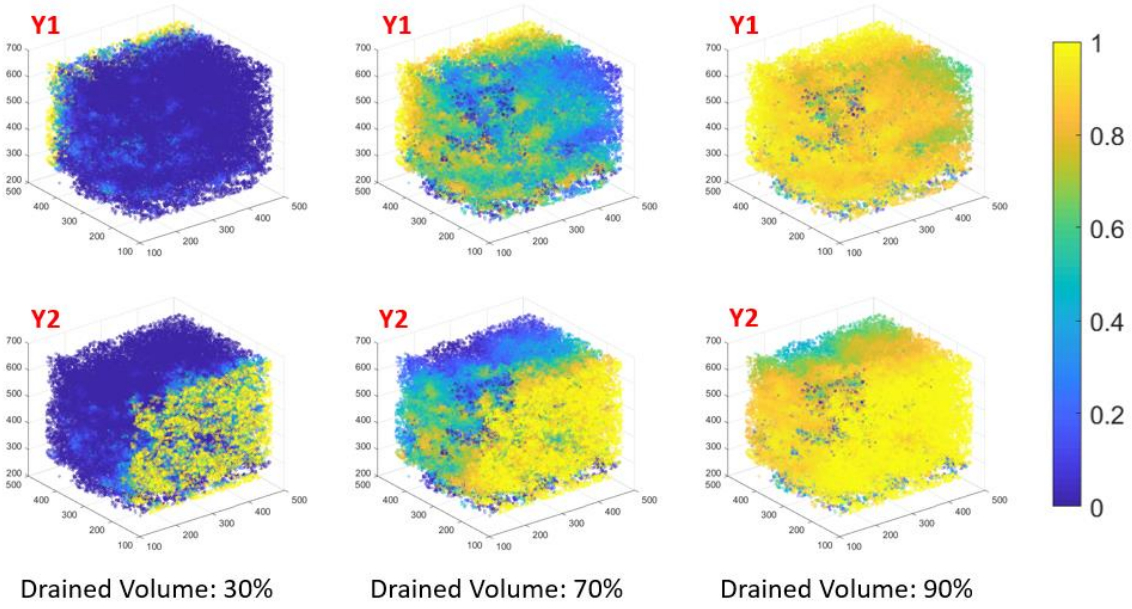

Fig. 46 – Comparison of the Two Y-Direction Faces' Anisotropy for the Carbonate Model

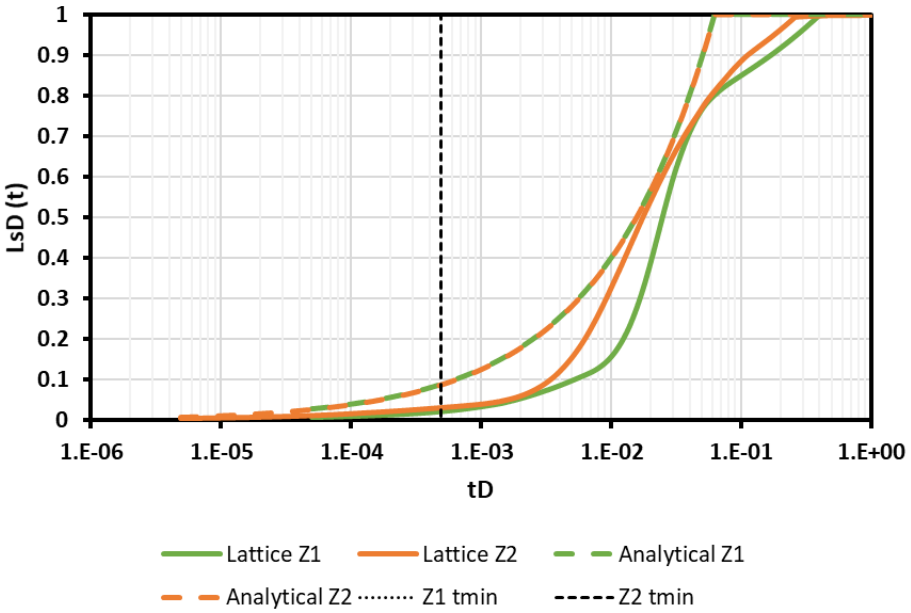

Fig. 47 – LsD Comparison Between Lattice and Analytical for the Two Faces in the Z Direction of the Carbonate Pore Network

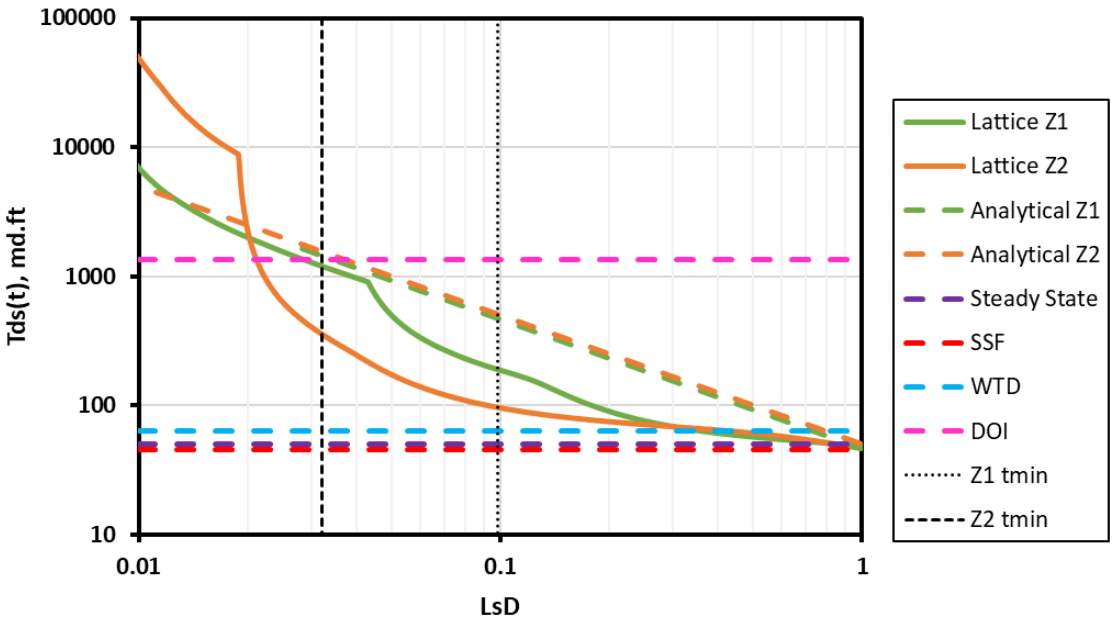

Fig. 48 – Transmissibility Comparison for the Two Faces in the Z Direction of the Carbonate Pore Network

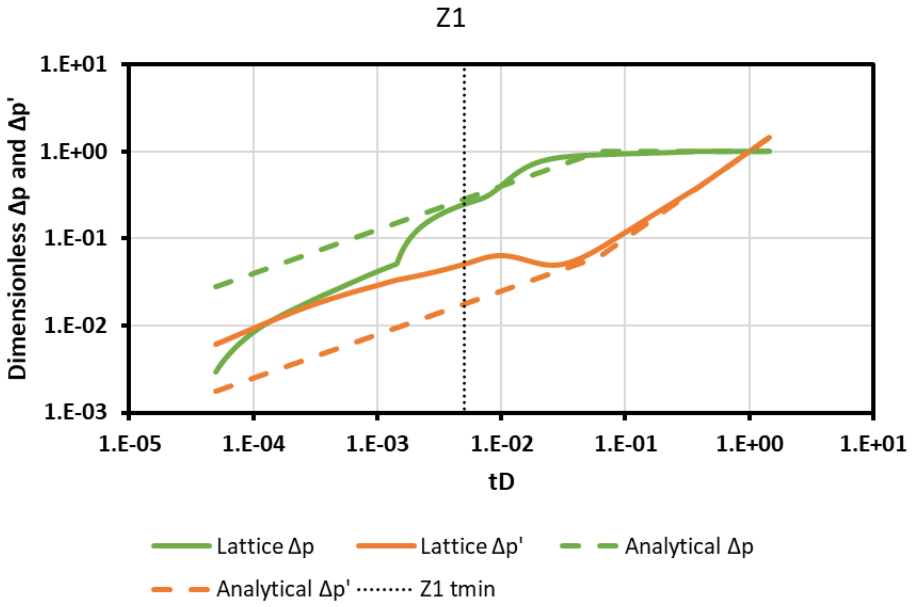

Fig. 49 – Diagnostic Plot for the Z1 Face of the Carbonate Pore Network

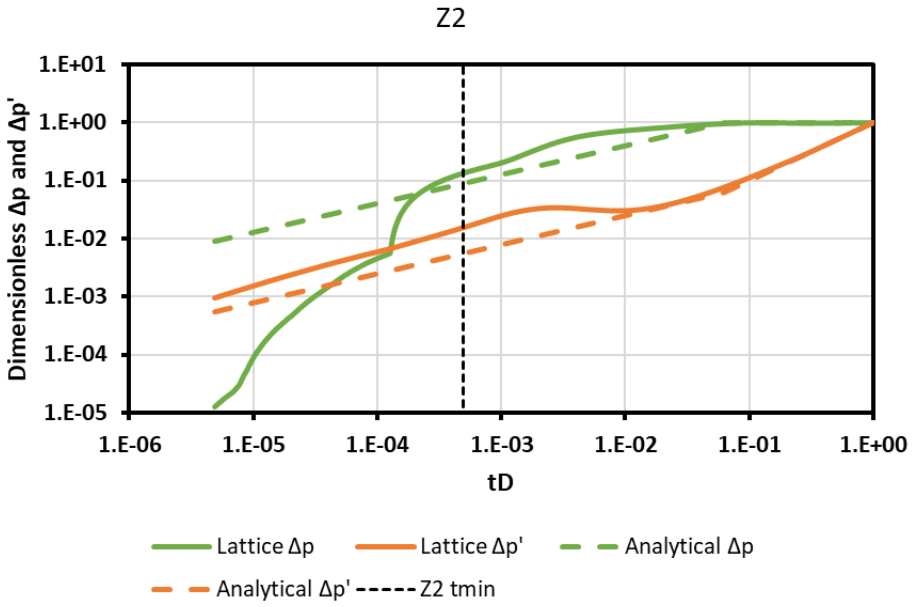

Fig. 50 – Diagnostic Plot for the Z2 Face of the Carbonate Pore Network

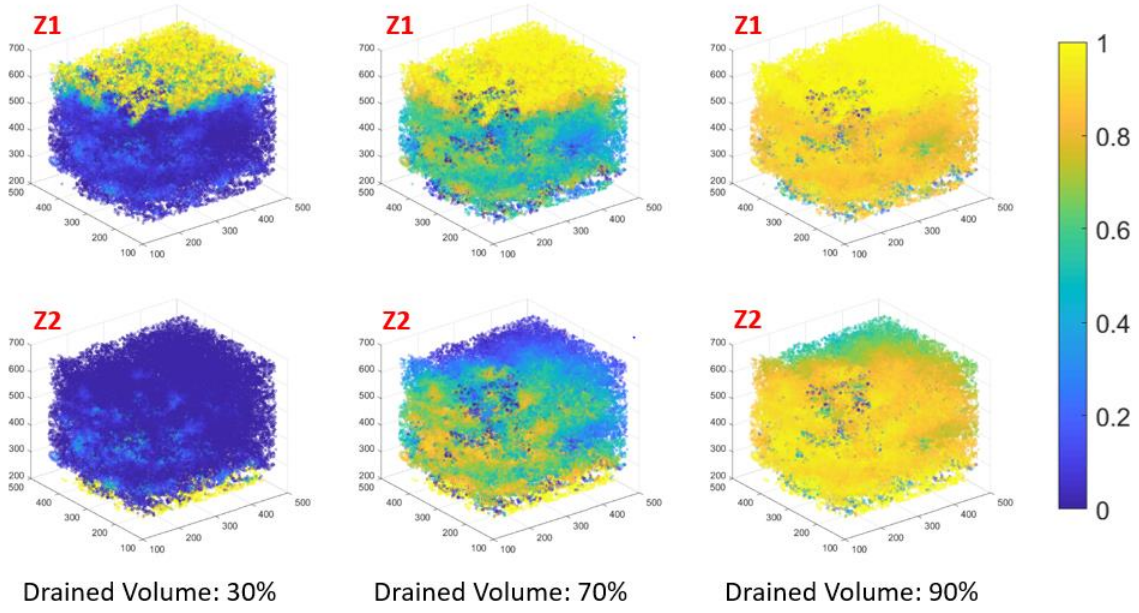

Fig. 51 – Comparison of the Two Z-Direction Faces' Anisotropy for the Carbonate Model